

# High energy particles from $\gamma$ -ray bursts\*

Eli Waxman

Weizmann Institute of Science, Rehovot 76100, Israel

**Abstract.** A review is presented of the fireball model of  $\gamma$ -ray bursts (GRBs), and of the production in GRB fireballs of high energy protons and neutrinos. Constraints imposed on the model by recent afterglow observations, which support the association of GRB and ultra-high energy cosmic-ray (UHECR) sources, are discussed. Predictions of the GRB model for UHECR production, which can be tested with planned large area UHECR detectors and with planned high energy neutrino telescopes, are reviewed. PACS numbers: 98.70.Rz, 98.70.Sa, 96.40.Tv, 14.60.Pq

## 1 Introduction and summary

The widely accepted interpretation of the phenomenology of  $\gamma$ -ray bursts (GRBs), bursts of 0.1 MeV–1 MeV photons lasting for a few seconds (see [32] for review), is that the observable effects are due to the dissipation of the kinetic energy of a relativistically expanding wind, a “fireball,” whose primal cause is not yet known (see [69,84] for reviews). The recent detection of “afterglows,” delayed low energy (X-ray to radio) emission of GRBs (see [61] for review), confirmed the cosmological origin of the bursts, through the redshift determination of several GRB host-galaxies, and confirmed standard model predictions of afterglows that result from the collision of an expanding fireball with its surrounding medium (see [70] for review). In this review, the production in GRB fireballs of  $\gamma$ -rays, high-energy cosmic-rays and neutrinos is discussed in the light of recent GRB and ultra-high-energy cosmic-ray observations.

The fireball model is described in detail in §2. We do not discuss in this section the issue of GRB progenitors, i.e. the underlying sources producing the relativistic fireballs. At present, the two leading progenitor scenarios are collapses of massive stars [36,81], and mergers of compact objects [42,79]. As explained in §2, the evolution of the fireball and the emission of  $\gamma$ -rays and afterglow radiation (on time scale of a day and longer) are largely independent of the nature of the progenitor. Thus, although present observations provide stringent constraints on the fireball model, the underlying progenitors remain unknown (e.g. [66]; see [61,70] for discussion). In §3, constraints imposed on the fireball model by recent afterglow observations are discussed, which are of importance for high energy particle production.

---

\* Based on lectures given at the *ICTP Summer School on Astroparticle Physics and Cosmology* (ICTP, Trieste Italy, June 2000), and at the *VI Gleb Wataghin School on High Energy Phenomenology* (UNICAMP, Campinas Brazil, July 2000).

The association of GRBs and ultra-high energy cosmic-rays (UHECRs) is discussed in §4. Recent afterglow observations strengthen the evidence for GRB and UHECR association, which is based on two key points (see [108] for recent review). First, the constraints imposed on fireball model parameters by recent observations imply that acceleration of protons is possible to energy higher than previously assumed,  $\sim 10^{21}$  eV. Second, the inferred local ( $z = 0$ ) GRB energy generation rate of  $\gamma$ -rays,  $\sim 10^{44}$  erg/Mpc<sup>3</sup>yr, is remarkably similar to the local generation rate of UHECRs implied by cosmic-ray observations.

The GRB model for UHECR production makes unique predictions, that may be tested with operating and planned large area UHECR detectors [23,25,103,97]. These predictions are described in §5. In particular, a critical energy is predicted to exist,  $10^{20}$  eV  $\leq \epsilon_c < 4 \times 10^{20}$  eV, above which a few sources produce most of the UHECR flux, and the observed spectra of these sources is predicted to be narrow,  $\Delta\epsilon/\epsilon \sim 1$ : the bright sources at high energy should be absent in UHECRs of much lower energy, since particles take longer to arrive the lower their energy. If the sources predicted by this model are detected by planned large area UHECR detectors, this would not only confirm the GRB model for UHECR production, but will also provide constraints on the unknown structure and strength of the inter-galactic magnetic field.

We note, that the AGASA experiment has recently reported the presence of one triplet and 3 doublets of UHECR events above  $4 \times 10^{19}$  eV, with angular separations (within each group)  $\leq 2.5^\circ$ , roughly consistent with the measurement error [96]. The probability that these multiplets are chance coincidences (as opposed to being produced by point sources) is  $\sim 1\%$ . Therefore, this observation favors the bursting source model, although more data are needed to confirm it. Testing the predictions of the fireball model for UHECR production would require an exposure 10 times larger than that of present experiments. Such increase is expected to be provided by the HiRes [23] and Auger [25,103] detectors, and by the proposed Telescope Array detector [97].

Predictions for the emission of high energy neutrinos from GRB fireballs are discussed in §6. Implications for planned high energy neutrino telescopes (the ICECUBE extension of AMANDA, ANTARES, NESTOR; see [46] for review) are discussed in detail in §6.4. It is shown that the predicted flux of  $\geq 10^{14}$  eV neutrinos may be detectable by Cerenkov neutrino telescopes while the flux above  $10^{19}$  eV may be detectable by large air-shower detectors [19,65,94]. Detection of the predicted neutrino signal will confirm the GRB fireball model for UHECR production and may allow to discriminate between different fireball progenitor scenarios. Moreover, a detection of even a handful of neutrino events correlated with GRBs will allow to test for neutrino properties, e.g. flavor oscillation and coupling to gravity, with accuracy many orders of magnitude better than currently possible.

## 2 The Fireball model

## 2.1 Relativistic expansion

General phenomenological considerations, based on  $\gamma$ -ray observations, indicate that, regardless of the nature of the underlying sources, GRBs are produced by the dissipation of the kinetic energy of a relativistic expanding fireball. The rapid rise time and short duration,  $\sim 1$  ms, observed in some bursts [11,31] imply that the sources are compact, with a linear scale comparable to a light-ms,  $r_0 \sim 10^7$  cm. The high  $\gamma$ -ray luminosity implied by cosmological distances,  $L_\gamma \sim 10^{52}$  erg s $^{-1}$ , then results in a very high optical depth to pair creation. The energy of observed  $\gamma$ -ray photons is above the threshold for pair production. The number density of photons at the source  $n_\gamma$  is approximately given by  $L_\gamma = 4\pi r_0^2 c n_\gamma \epsilon$ , where  $\epsilon \simeq 1$  MeV is the characteristic photon energy. Using  $r_0 \sim 10^7$  cm, the optical depth for pair production at the source is

$$\tau_{\gamma\gamma} \sim r_0 n_\gamma \sigma_T \sim \frac{\sigma_T L_\gamma}{4\pi r_0 c \epsilon} \sim 10^{15}, \quad (1)$$

where  $\sigma_T$  is the Thomson cross section.

The high optical depth implies that a thermal plasma of photons, electrons and positrons is created, a ‘‘fireball,’’ which then expands and accelerates to relativistic velocities [79,42]. The optical depth is reduced by relativistic expansion of the source: If the source expands with a Lorentz factor  $\Gamma$ , the energy of photons in the source frame is smaller by a factor  $\Gamma$  compared to that in the observer frame, and most photons may therefore be below the pair production threshold.

A lower limit for  $\Gamma$  may be obtained in the following way [57,9]. The GRB photon spectrum is well fitted in the Burst and Transient Source Experiment (BATSE) detectors range, 20 keV to 2 MeV [32], by a combination of two power-laws,  $dn_\gamma/d\epsilon_\gamma \propto \epsilon_\gamma^{-\beta}$  with different values of  $\beta$  at low and high energy [8]. Here,  $dn_\gamma/d\epsilon_\gamma$  is the number of photons per unit photon energy. The break energy (where  $\beta$  changes) in the observer frame is typically  $\epsilon_{\gamma b} \sim 1$  MeV, with  $\beta \simeq 1$  at energies below the break and  $\beta \simeq 2$  above the break. In several cases, the spectrum was observed to extend to energies  $> 100$  MeV [93,32]. Consider then a high energy test photon, with observed energy  $\epsilon_t$ , trying to escape the relativistically expanding source. Assuming that in the source rest frame the photon distribution is isotropic, and that the spectrum of high energy photons follows  $dn_\gamma/d\epsilon_\gamma \propto \epsilon_\gamma^{-2}$ , the mean free path for pair production (in the source rest frame) for a photon of energy  $\epsilon'_t = \epsilon_t/\gamma$  (in the source rest frame) is

$$l_{\gamma\gamma}^{-1}(\epsilon'_t) = \frac{1}{2} \frac{3}{16} \sigma_T \int d\cos\theta (1 - \cos\theta) \int_{\epsilon_{\text{th}}(\epsilon'_t, \theta)}^{\infty} d\epsilon \frac{U_\gamma}{2\epsilon^2} = \frac{1}{16} \sigma_T \frac{U_\gamma \epsilon'_t}{(m_e c^2)^2}. \quad (2)$$

Here,  $\epsilon_{\text{th}}(\epsilon'_t, \theta)$  is the minimum energy of photons that may produce pairs interacting with the test photon, given by  $\epsilon_{\text{th}} \epsilon'_t (1 - \cos\theta) \geq 2(m_e c^2)^2$  ( $\theta$  is the angle between the photons' momentum vectors).  $U_\gamma$  is the photon energy density (in the range corresponding to the observed BATSE range) in the source rest-frame, given by  $L_\gamma = 4\pi r^2 \gamma^2 c U_\gamma$ . Note, that we have used a constant cross section,

$3\sigma_T/16$ , above the threshold  $\epsilon_{\text{th}}$ . The cross section drops as  $\log(\epsilon)/\epsilon$  for  $\epsilon \gg \epsilon_{\text{th}}$ ; however, since the number density of photons drops rapidly with energy, this does not introduce a large correction to  $l_{\gamma\gamma}$ .

The source size constraint implied by the variability time is modified for a relativistically expanding source. Since in the observer frame almost all photons propagate at a direction making an angle  $< 1/\Gamma$  with respect to the expansion direction, radiation seen by a distant observer originates from a conical section of the source around the source-observer line of sight, with opening angle  $\sim 1/\Gamma$ . Photons which are emitted from the edge of the cone are delayed, compared to those emitted on the line of sight, by  $r/2\Gamma^2 c$ . Thus, the constraint on source size implied by variability on time scale  $\Delta t$  is

$$r \sim 2\Gamma^2 c \Delta t. \quad (3)$$

The time  $r/c$  required for significant source expansion corresponds to comoving time (measured in the source frame)  $t_{\text{co.}} \approx r/\Gamma c$ . The two-photon collision rate at the source frame is  $t_{\gamma\gamma}^{-1} = c/l_{\gamma\gamma}$ . Thus, the source optical depth to pair production is  $\tau_{\gamma\gamma} = t_{\text{co.}}/t_{\gamma\gamma} \approx r/\Gamma l_{\gamma\gamma}$ . Using Eqs. (2) and (3) we have

$$\tau_{\gamma\gamma} = \frac{1}{128\pi} \frac{\sigma_T L_\gamma \epsilon_t}{c^2 (m_e c^2)^2 \Gamma^6 \Delta t}. \quad (4)$$

Requiring  $\tau_{\gamma\gamma} < 1$  at  $\epsilon_t$  we obtain a lower limit for  $\Gamma$ ,

$$\Gamma \geq 250 \left[ L_{\gamma,52} \left( \frac{\epsilon_t}{100 \text{ MeV}} \right) \Delta t_{-2}^{-1} \right]^{1/6}, \quad (5)$$

where  $L_\gamma = 10^{52} L_{\gamma,52} \text{ erg/s}$  and  $\Delta t = 10^{-2} \Delta t_{-2} \text{ s}$ .

## 2.2 Fireball evolution

As the fireball expands it cools, the photon temperature  $T_\gamma$  in the fireball frame decreases, and most pairs annihilate. Once the pair density is sufficiently low, photons may escape. However, if the observed radiation is due to photons escaping the fireball as it becomes optically thin, two problems arise. First, the photon spectrum is quasi-thermal, in contrast with observations. Second, the source size,  $r_0 \sim 10^7 \text{ cm}$ , and the total energy emitted in  $\gamma$ -rays,  $\sim 10^{53} \text{ erg}$ , suggest that the underlying energy source is related to the gravitational collapse of  $\sim 1M_\odot$  object. Thus, the plasma is expected to be ‘‘loaded’’ with baryons which may be injected with the radiation or present in the atmosphere surrounding the source. A small baryonic load,  $\geq 10^{-8} M_\odot$ , increases the optical depth due to Thomson scattering on electrons associated with the ‘‘loading’’ protons, so that most of the radiation energy is converted to kinetic energy of the relativistically expanding baryons before the plasma becomes optically thin [80,91]. To overcome both problems it was proposed [87] that the observed burst is produced once the kinetic energy of the ultra-relativistic ejecta is re-randomized by some dissipation process at large radius, beyond the Thomson photosphere, and

then radiated as γ-rays. Collision of the relativistic baryons with the inter-stellar medium [87], and internal collisions within the ejecta itself [78,83,71], were proposed as possible dissipation processes. Most GRBs show variability on time scales much shorter than (typically one hundredth of) the total GRB duration. Such variability is hard to explain in models where the energy dissipation is due to external shocks [117,88]. Thus, it is believed that internal collisions are responsible for the emission of γ-rays.

Let us first consider the case where the energy release from the source is “instantaneous,” i.e. on a time scale  $r_0/c$ . We assume that most of the energy is released in the form of photons, i.e. that the fraction of energy carried by baryon rest mass  $M$  satisfies  $\eta^{-1} \equiv Mc^2/E \ll 1$ . The initial thickness of the fireball shell is  $r_0$ . Since the plasma accelerates to relativistic velocity, all fluid elements move with velocity close to  $c$ , and the shell thickness remains constant at  $r_0$  (this breaks at very late time, as discussed below). We are interested in the stage where the optical depth (due to pairs and/or electrons associated with baryons) is high, but only a small fraction of the energy is carried by pairs.

The entropy of a fluid component with zero chemical potential is  $S = V(e + p)/T$ , where  $e$ ,  $p$  and  $V$  are the (rest frame) energy density, pressure and volume. For the photons  $p = e/3 \propto T_\gamma^4$ . Since initially both the rest mass and thermal energy of baryons is negligible, the entropy is provided by the photons. Conservation of entropy implies

$$r^2\gamma(r)r_0T_\gamma^3(r) = \text{Constant}, \tag{6}$$

and conservation of energy implies

$$r^2\gamma(r)r_0\gamma(r)T_\gamma^4(r) = \text{Constant}. \tag{7}$$

Here  $\gamma(r)$  is the shell Lorentz factor. Combining (6) and (7) we find

$$\gamma(r) \propto r, \quad T_\gamma(r) \propto r^{-1}, \quad n \propto r^{-3}, \tag{8}$$

where  $n$  is the rest frame (comoving) baryon number density.

As the shell accelerates the baryon kinetic energy,  $\gamma Mc^2$ , increases. It becomes comparable to the total fireball energy when  $\gamma \sim \eta$ , at radius  $r_f = \eta r_0$ . At this radius most of the energy of the fireball is carried by the baryon kinetic energy, and the shell does not accelerate further. Eq. (7) describing energy conservation is replaced with  $\gamma = \text{Constant}$ . Eq. (6), however, still holds. Eq. (6) may be written as  $T_\gamma^4/nT_\gamma = \text{Constant}$  (constant entropy per baryon). This implies that the ratio of radiation energy density to thermal energy density associated with the baryons is  $r$  independent. Thus, the thermal energy associated with the baryons may be neglected at all times, and Eq. (6) holds also for the stage where most of the fireball energy is carried by the baryon kinetic energy. Thus, for  $r > r_f$  we have

$$\gamma(r) = \Gamma \approx \eta, \quad T \propto r^{-2/3}, \quad n \propto r^{-2}. \tag{9}$$

Let us consider now the case of extended emission from the source, on time scale  $\gg r_0/c$ . In this case, the source continuously emits energy at a rate  $L$ , and

the energy emission is accompanied by mass loss rate  $\dot{M} = L/\eta c^2$ . For  $r < r_f$  the fluid energy density is relativistic,  $aT_\gamma^4/nm_p c^2 = \eta r_0/r$ , and the speed of sound is  $\sim c$ . The time it takes the shell at radius  $r$  to expand significantly is  $r/c$  in the observer frame, corresponding to  $t_{\text{co.}} \sim r/\gamma c$  in the shell frame. During this time sound waves can travel a distance  $cr/\gamma c$  in the shell frame, corresponding to  $r/\gamma^2 = r/(r/r_0)^2 = (r_0/r)r_0$  in the observer frame. This implies that at the early stages of evolution,  $r \sim r_0$ , sound waves had enough time to smooth out spatial fluctuations in the fireball over a scale  $r_0$ , but that regions separated by  $\Delta r > r_0$  can not interact with each other. Thus, if the emission extends over a time  $T_{\text{GRB}} \gg r_0/c$ , a fireball of thickness  $cT_{\text{GRB}} \gg r_0$  would be formed, which would expand as a collection of independent, roughly uniform, sub-shells of thickness  $r_0$ . Each sub-shell would reach a final Lorentz factor  $\Gamma_f$ , which may vary between sub-shells. This implies that different sub-shells may have velocities differing by  $\Delta v \sim c/2\eta^2$ , where  $\eta$  is some typical value representative of the entire fireball. Different shells emitted at times differing by  $\Delta t$ ,  $r_0/c < \Delta t < T_{\text{GRB}}$ , may therefore collide with each other after a time  $t_c \sim c\Delta t/\Delta v$ , i.e. at a radius

$$r_i \approx 2\Gamma^2 c\Delta t = 6 \times 10^{13} \Gamma_{2.5}^2 \Delta t_{-2} \text{ cm}, \quad (10)$$

where  $\Gamma = 10^{2.5} \Gamma_{2.5}$ . The minimum internal shock radius,  $r \sim \Gamma^2 r_0$ , is also the radius at which an individual sub-shell may experience significant change in its width  $r_0$ , due to Lorentz factor variation across the shell.

### 2.3 The allowed range of Lorentz factors and baryon loading

The acceleration,  $\gamma \propto r$ , of fireball plasma is driven by radiation pressure. Fireball protons are accelerated through their coupling to the electrons, which are coupled to fireball photons. We have assumed in the analysis presented above, that photons and electrons are coupled throughout the acceleration phase. However, if the baryon loading is too low, radiation may decouple from fireball electrons already at  $r < r_f$ . The fireball Thomson optical depth is given by the product of comoving expansion time,  $r/\gamma(r)c$ , and the photon Thomson scattering rate,  $n_e c\sigma_T$ . The electron and proton comoving number densities are equal,  $n_e = n_p$ , and are determined by equating the  $r$  independent mass flux carried by the wind,  $4\pi r^2 c\gamma(r)n_p m_p$ , to the mass loss rate from the underlying source, which is related to the rate  $L$  at which energy is emitted through  $\dot{M} = L/(\eta c^2)$ . Thus, during the acceleration phase,  $\gamma(r) = r/r_0$ , the Thomson optical depth  $\tau_T \propto r^{-3}$ .  $\tau_T$  drops below unity at a radius  $r < r_f = \eta r_0$  if  $\eta > \eta_*$ , where

$$\eta_* = \left( \frac{\sigma_T L}{4\pi r_0 m_p c^3} \right)^{1/4} = 1.0 \times 10^3 L_{52}^{1/4} r_{0,7}^{-1/4}. \quad (11)$$

Here  $r_0 = 10^7 r_{0,7}$  cm.

If  $\eta > \eta_*$  radiation decouples from the fireball plasma at  $\gamma = r/r_0 = \eta_*^{4/3} \eta^{-1/3}$ . If  $\eta \gg \eta_*$ , then most of the radiation energy is not converted to kinetic energy prior to radiation decoupling, and most of the fireball energy

escapes in the form of thermal radiation. Thus, the baryon load of fireball shells, and the corresponding final Lorentz factors, must be within the range  $10^2 \leq \Gamma \approx \eta \leq \eta_* \approx 10^3$  in order to allow the production of the observed non-thermal γ-ray spectrum.

## 2.4 Fireball interaction with surrounding medium

As the fireball expands, it drives a relativistic shock (blast-wave) into the surrounding gas, e.g. into the inter-stellar medium (ISM) gas if the explosion occurs within a galaxy. In what follows, we refer to the surrounding gas as “ISM gas,” although the gas need not necessarily be inter-stellar. At early time, the fireball is little affected by the interaction with the ISM. At late time, most of the fireball energy is transferred to the ISM, and the flow approaches the self-similar blast-wave solution of Blandford & McKee [15]. At this stage a single shock propagates into the ISM, behind which the gas expands with Lorentz factor

$$\Gamma_{BM}(r) = \left( \frac{17E}{16\pi n m_p c^2} \right)^{1/2} r^{-3/2} = 150 \left( \frac{E_{53}}{n_0} \right)^{1/2} r_{17}^{-3/2}, \quad (12)$$

where  $E = 10^{53} E_{53}$  erg is the fireball energy,  $n = 1 n_0 \text{ cm}^{-3}$  is the ISM number density, and  $r = 10^{17} r_{17}$  cm is the shell radius. The characteristic time at which radiation emitted by shocked plasma at radius  $r$  is observed by a distant observer is  $t \approx r/4\Gamma_{BM}^2 c$  [107].

The transition to self-similar expansion occurs on a time scale  $T$  (measured in the observer frame) comparable to the longer of the two time scales set by the initial conditions: the (observer) GRB duration  $T_{\text{GRB}}$  and the (observer) time  $T_\Gamma$  at which the self-similar Lorentz factor equals the original ejecta Lorentz factor  $\Gamma$ ,  $\Gamma_{BM}(t = T_\Gamma) = \Gamma$ . Since  $t = r/4\Gamma_{BM}^2 c$ ,

$$T = \max \left[ T_{\text{GRB}}, 5 \left( \frac{E_{53}}{n_0} \right)^{1/3} \Gamma_{2.5}^{-8/3} \text{ s} \right]. \quad (13)$$

During the transition, plasma shocked by the reverse shocks expands with Lorentz factor close to that given by the self-similar solution,

$$\Gamma_{\text{tr.}} \simeq \Gamma_{BM}(t = T) \simeq 245 \left( \frac{E_{53}}{n_0} \right)^{1/8} T_1^{-3/8}, \quad (14)$$

where  $T = 10T_1$  s. The unshocked fireball ejecta propagate at the original expansion Lorentz factor,  $\Gamma$ , and the Lorentz factor of plasma shocked by the reverse shock in the rest frame of the unshocked ejecta is  $\simeq \Gamma/\Gamma_{\text{tr.}}$ . If  $T \simeq T_{\text{GRB}} \gg T_\Gamma$  then  $\Gamma/\Gamma_{\text{tr.}} \gg 1$ , the reverse shock is relativistic, and the Lorentz factor associated with the random motion of protons in the reverse shock is  $\gamma_p^R \simeq \Gamma/\Gamma_{\text{tr.}}$ .

If, on the other hand,  $T \simeq T_\Gamma \gg T_{\text{GRB}}$  then  $\Gamma/\Gamma_{\text{tr.}} \sim 1$ , and the reverse shock is not relativistic. Nevertheless, the following argument suggests that the reverse shock speed is not far below  $c$ , and that the protons are therefore heated

to relativistic energy,  $\gamma_p^R - 1 \simeq 1$ . The comoving time, measured in the fireball ejecta frame prior to deceleration, is  $t_{\text{co.}} \simeq r/\Gamma c$ . The expansion Lorentz factor is expected to vary across the ejecta,  $\Delta\Gamma/\Gamma \sim 1$ , due to variability of the underlying GRB source over the duration of its energy release. Such variation would lead to expansion of the ejecta, in the comoving frame, at relativistic speed. Thus, at the deceleration radius,  $t_{\text{co.}} \simeq \Gamma T$ , the ejecta width exceeds  $\simeq ct_{\text{co.}} \simeq \Gamma cT$ . Since the reverse shock should cross the ejecta over a deceleration time scale,  $\simeq \Gamma T$ , the reverse shock speed must be close to  $c$ . We therefore conclude that the Lorentz factor associated with the random motion of protons in the reverse shock is approximately given by  $\gamma_p^R - 1 \simeq \Gamma/\Gamma_{\text{tr.}}$  for both  $\Gamma/\Gamma_{\text{tr.}} \sim 1$  and  $\Gamma/\Gamma_{\text{tr.}} \gg 1$ .

Since  $T_{\text{GRB}} \sim 10$  s is typically comparable to  $T_\Gamma$ , the reverse shocks are typically expected to be mildly relativistic.

## 2.5 Fireball geometry

We have assumed in the discussion so far that the fireball is spherically symmetric. However, a jet-like fireball behaves as if it were a conical section of a spherical fireball as long as the jet opening angle is larger than  $\Gamma^{-1}$ . This is due to the fact that the linear size of causally connected regions,  $ct_{\text{co.}} \sim r/\Gamma$  in the fireball frame, corresponds to an angular size  $ct_{\text{co.}}/r \sim \Gamma^{-1}$ . Moreover, due to the relativistic beaming of radiation, a distant observer can not distinguish between a spherical fireball and a jet-like fireball, as long as the jet opening angle  $\theta > \Gamma^{-1}$ . Thus, as long as we are discussing processes that occur when the wind is ultra-relativistic,  $\Gamma \sim 300$  (prior to significant fireball deceleration by the surrounding medium), our results apply for both a spherical and a jet-like fireball. In the latter case,  $L(E)$  in our equations should be understood as the luminosity (energy) the fireball would have carried had it been spherically symmetric.

## 2.6 $\gamma$ -ray emission

If the Lorentz factor variability within the wind is significant, internal shocks would reconvert a substantial part of the kinetic energy to internal energy. The internal energy may then be radiated as  $\gamma$ -rays by synchrotron and inverse-Compton emission of shock-accelerated electrons. The internal shocks are expected to be “mildly” relativistic in the fireball rest frame, i.e. characterized by Lorentz factor  $\Gamma_i - 1 \sim$  a few. This is due to the fact that the allowed range of shell Lorentz factors is  $\sim 10^2$  to  $\sim 10^3$  (see §2.3), implying that the Lorentz factors associated with the relative velocities are not very large. Since internal shocks are mildly relativistic, we expect results related to particle acceleration in sub-relativistic shocks (see [14] for review) to be valid for acceleration in internal shocks. In particular, electrons are expected to be accelerated to a power law energy distribution,  $dn_e/d\gamma_e \propto \gamma_e^{-p}$  for  $\gamma_e > \gamma_m$ , with  $p \simeq 2$  [4,10,16].

The minimum Lorentz factor  $\gamma_m$  is determined by the following consideration. Protons are heated in internal shocks to random velocities (in the wind



frame)  $\gamma_p^R - 1 \approx \Gamma_i - 1 \approx 1$ . If electrons carry a fraction  $\xi_e$  of the shock internal energy, then  $\gamma_m \approx \xi_e(m_p/m_e)$ . The characteristic frequency of synchrotron emission is determined by  $\gamma_m$  and by the strength of the magnetic field. Assuming that a fraction  $\xi_B$  of the internal energy is carried by the magnetic field,  $4\pi r_i^2 c \Gamma^2 B^2 / 8\pi = \xi_B L_{\text{int.}}$ , the characteristic observed energy of synchrotron photons,  $\epsilon_{\gamma b} = \Gamma \hbar \gamma_m^2 e B / m_e c$ , is

$$\epsilon_{\gamma b} \approx 1 \xi_B^{1/2} \xi_e^{3/2} \frac{L_{\gamma,52}^{1/2}}{\Gamma_{2.5}^2 \Delta t_{-2}} \text{MeV}. \quad (15)$$

In deriving Eq. (15) we have assumed that the wind luminosity carried by internal plasma energy,  $L_{\text{int.}}$ , is related to the observed  $\gamma$ -ray luminosity through  $L_{\text{int.}} = L_\gamma / \xi_e$ . This assumption is justified since the electron synchrotron cooling time is short compared to the wind expansion time (unless the equipartition fraction  $\xi_B$  is many orders of magnitude smaller than unity), and hence electrons lose all their energy radiatively. Fast electron cooling also results in a synchrotron spectrum  $dn_\gamma/d\epsilon_\gamma \propto \epsilon_\gamma^{-1-p/2} = \epsilon_\gamma^{-2}$  at  $\epsilon_\gamma > \epsilon_{\gamma b}$ , consistent with observed GRB spectra [8].

At present, there is no theory that allows the determination of the values of the equipartition fractions  $\xi_e$  and  $\xi_B$ . Eq. (15) implies that fractions not far below unity are required to account for the observed  $\gamma$ -ray emission. We note, that build up of magnetic field to near equipartition by electro-magnetic instabilities is expected to be a generic characteristic of collisionless shocks (see discussion in ref. [14] and references therein), and is inferred to occur in other systems, e.g. in supernova remnant shocks (e.g. [50,20]).

The  $\gamma$ -ray break energy  $\epsilon_{\gamma b}$  of most GRBs observed by BATSE detectors is in the range of 100 keV to 300 keV [18]. It may appear from Eq. (15) that the clustering of break energies in this narrow energy range requires fine tuning of fireball model parameters, which should naturally produce a much wider range of break energies. This is, however, not the case [44]. Consider the dependence of  $\epsilon_{\gamma b}$  on  $\Gamma$ . The strong  $\Gamma$  dependence of the pair-production optical depth, Eq. (4), implies that if the value of  $\Gamma$  is smaller than the minimum value allowed by Eq. (5), for which  $\tau_{\gamma\gamma}(\epsilon_\gamma = 100\text{MeV}) \approx 1$ , most of the high energy photons in the power-law distribution produced by synchrotron emission,  $dn_\gamma/d\epsilon_\gamma \propto \epsilon_\gamma^{-2}$ , would be converted to pairs. This would lead to high optical depth due to Thomson scattering on  $e^\pm$ , and hence to strong suppression of the emitted flux [44]. For fireball parameters such that  $\tau_{\gamma\gamma}(\epsilon_\gamma = 100\text{MeV}) \approx 1$ , the break energy implied by Eqs. (15) and (5) is

$$\epsilon_{\gamma b} \approx 1 \xi_B^{1/2} \xi_e^{3/2} \frac{L_{\gamma,52}^{1/6}}{\Delta t_{-2}^{2/3}} \text{MeV}. \quad (16)$$

As explained in §2.3, shell Lorentz factors can not exceed  $\eta_* \simeq 10^3$ , for which break energies in the X-ray range,  $\epsilon_{\gamma b} \sim 10$  keV, may be obtained. We note, however, that the radiative flux would be strongly suppressed in this case too [44]. If the typical  $\Gamma$  of radiation emitting shells is close to  $\eta_*$ , then the range

of Lorentz factors of wind shells is narrow, which implies that only a small fraction of wind kinetic energy would be converted to internal energy which can be radiated from the fireball.

Thus, the clustering of break energies at  $\sim 1$  MeV is naturally accounted for, provided that the variability time scale satisfies  $\Delta t \leq 10^{-2}$  s, which implies an upper limit on the source size, since  $\Delta t \geq r_0/c$ . We note, that a large fraction of bursts detected by BATSE show variability on the shortest resolved time scale,  $\sim 10$  ms [117]. In addition, a natural consequence of the model is the existence of low luminosity bursts with low, 1 keV to 10 keV, break energies [44]. Such “X-ray bursts” may have recently been identified [55].

For internal collisions, the observed  $\gamma$ -ray variability time,  $\sim r_i/\Gamma^2 c \approx \Delta t$ , reflects the variability time of the underlying source, and the GRB duration reflects the duration over which energy is emitted from the source. Since the wind Lorentz factor is expected to fluctuate on time scales ranging from the shortest variability time  $r_0/c$  to the wind duration  $T_{\text{GRB}}$ , internal collisions will take place over a range of radii,  $r \sim \Gamma^2 r_0$  to  $r \sim \Gamma^2 c T_{\text{GRB}}$ .

## 2.7 Afterglow emission

Let us consider the radiation emitted from the reverse shocks, during the transition to self-similar expansion. The characteristic electron Lorentz factor (in the plasma rest frame) is  $\gamma_m \simeq \xi_e(\Gamma/\Gamma_{\text{tr}})m_p/m_e$ , where the internal energy per proton in the shocked ejecta is  $\simeq (\Gamma/\Gamma_{\text{tr}})m_p c^2$ . The energy density  $U$  is  $E \approx 4\pi r^2 c T \Gamma_{\text{tr}}^2 U$ , and the number of radiating electrons is  $N_e \approx E/\Gamma m_p c^2$ . Using Eq. (14) and  $r = 4\Gamma_{\text{tr}}^2 c T$ , the characteristic (or peak) energy of synchrotron photons (in the observer frame) is [113]

$$\epsilon_{\gamma m} \approx \hbar \Gamma_{\text{tr}} \gamma_m^2 \frac{eB}{m_e c} = 2\xi_{e,-1}^2 \xi_{B,-1}^{1/2} n_0^{1/2} \Gamma_{2.5}^2 \text{ eV}, \quad (17)$$

and the specific luminosity,  $L_\epsilon = dL/d\epsilon_\gamma$ , at  $\epsilon_{\gamma m}$  is

$$L_m \approx (2\pi\hbar)^{-1} \Gamma_{\text{tr}} \frac{e^3 B}{m_e c^2} N_e \approx 10^{61} \xi_{B,-1}^{1/2} E_{53}^{5/4} T_1^{-3/4} \Gamma_{2.5}^{-1} n_0^{1/4} \text{ s}^{-1}, \quad (18)$$

where  $\xi_e = 0.1\xi_{e,-1}$ , and  $\xi_B = 0.1\xi_{B,-1}$ .

Here too, we expect a power law energy distribution,  $dN_e/d\gamma_e \propto \gamma_e^{-p}$  for  $\gamma_e > \gamma_m$ , with  $p \simeq 2$ . Since the radiative cooling time of electrons in the reverse shock is long compared to the ejecta expansion time, the specific luminosity extends in this case to energy  $\epsilon_\gamma > \epsilon_{\gamma m}$  as  $L_\epsilon = L_m(\epsilon_\gamma/\epsilon_{\gamma m})^{-1/2}$ , up to photon energy  $\epsilon_{\gamma c}$ . Here  $\epsilon_{\gamma c}$  is the characteristic synchrotron frequency of electrons for which the synchrotron cooling time,  $6\pi m_e c/\sigma_T \gamma_e B^2$ , is comparable to the ejecta (rest frame) expansion time,  $\sim \Gamma_{\text{tr}} T$ . At energy  $\epsilon_\gamma > \epsilon_{\gamma c}$ ,

$$\epsilon_{\gamma c} \approx 0.1 \xi_{B,-1}^{-3/2} n_0^{-1} E_{53}^{-1/2} T_1^{-1/2} \text{ keV}, \quad (19)$$

the spectrum steepens to  $L_\epsilon \propto \epsilon_\gamma^{-1}$ .

The shock driven into the ISM continuously heats new gas, and produces relativistic electrons that may produce the delayed afterglow radiation observed on time scales  $t \gg T$ , typically of order days to months. As the shock-wave decelerates, the emission shifts to lower frequency with time. Since we are interested in proton acceleration to high energy and in the production of high energy neutrinos, which take place primarily in the internal and reverse shocks (see §4, §6), we do not discuss in detail the theory of late-time afterglow emission.

### 3 Some implications of afterglow observations

Afterglow observations lead to the confirmation, as mentioned in the Introduction, of the cosmological origin of GRBs [61], and confirmed [106,116] standard model predictions [82,54,72,100] of afterglow that results from synchrotron emission of electrons accelerated to high energy in the highly relativistic shock driven by the fireball into its surrounding gas. Since we are interested mainly in the earlier, internal collision phase of fireball evolution, we do not discuss afterglow observations in detail. We note, however, several implications of afterglow observations which are of importance for the discussion of UHECR production.

The following point should be clarified in the context of afterglow observations. The distribution of GRB durations is bimodal, with broad peaks at  $T_{\text{GRB}} = 0.2$  s and  $T_{\text{GRB}} = 20$  s [32]. The majority of bursts belong to the long duration,  $T_{\text{GRB}} \sim 20$  s, class. The detection of afterglow emission was made possible thanks to the accurate GRB positions provided on hour time scale by the *BeppoSAX* satellite [24]. Since the detectors on board this satellite trigger only on long bursts, afterglow observations are not available for the sub-population of short,  $T_{\text{GRB}} \sim 0.2$  s, bursts. Thus, while the discussion of the fireball model presented in §2, based on  $\gamma$ -ray observations and on simple phenomenological arguments, applies to both long and short duration bursts, the discussion below of afterglow observations applies to long duration bursts only. It should therefore be kept in mind that short duration bursts may constitute a different class of GRBs, which, for example, may be produced by a different class of progenitors and may have a different redshift distribution than the long duration bursts.

Prior to the detection of afterglows, it was commonly assumed that the farthest observed GRBs lie at redshift  $z \sim 1$ . Following the detection of afterglows and the determination of GRB redshifts, it is now clear that most GRB sources lie within the redshift range  $z \sim 0.5$  to  $z \sim 2$ , with some bursts observed at  $z > 3$ . For the average GRB  $\gamma$ -ray fluence,  $1.2 \times 10^{-5} \text{erg/cm}^2$  in the 20 keV to 2 MeV band, this implies characteristic isotropic  $\gamma$ -ray energy and luminosity  $E_\gamma \sim 10^{53}$  erg and  $L_\gamma \sim 10^{52}$  erg/s (in the 20 keV to 2 MeV band), about an order of magnitude higher than the values assumed prior to afterglow detection (Here, and throughout the paper we assume a flat universe with  $\Omega = 0.3$ ,  $\Lambda = 0.7$ , and  $H_0 = 65 \text{km/s Mpc}$ ). These estimates are consistent with more detailed analyses of the GRB luminosity function and redshift distribution. Mao & Mo, e.g., find, for the cosmological parameters we use, a median GRB energy

of  $\approx 0.6 \times 10^{53}$  erg in the 50 keV to 300 keV band [68], corresponding to a median GRB energy of  $\approx 2 \times 10^{53}$  erg in the 20 keV to 2 MeV band.

The determination of GRB redshifts also lead to a modification of GRB rate estimates. Since most observed GRB sources lie within the redshift range  $z \sim 0.5$  to  $z \sim 2$ , observations essentially determine the GRB rate per unit volume at  $z \sim 1$ . The observed rate of  $10^3/\text{yr}$  implies  $R_{\text{GRB}}(z = 1) \approx 3/\text{Gpc}^3\text{yr}$ . The present,  $z = 0$ , rate is less well constrained, since available data are consistent with both no evolution of GRB rate with redshift, and with strong evolution (following, e.g., star formation rate), in which  $R_{\text{GRB}}(z = 1)/R_{\text{GRB}}(z = 0) \sim 10$  [60,53]. Detailed analyses, assuming  $R_{\text{GRB}}$  is proportional to star formation rate, lead to  $R_{\text{GRB}}(z = 0) \sim 0.5/\text{Gpc}^3\text{yr}$  [61]. The implied local ( $z = 0$ )  $\gamma$ -ray energy generation rate by GRBs in the 20 keV to 2 MeV band is therefore

$$\dot{\epsilon}_\gamma(z = 0) = 10^{44}\zeta \text{ erg/Mpc}^3\text{yr}, \quad (20)$$

with  $\zeta$  in the range of  $\sim 10^{-0.5}$  to  $\sim 10^{0.5}$ . Note, that  $\dot{\epsilon}_\gamma$  is independent of the fireball geometry. If fireballs are conical jets of solid angle  $\Delta\Omega$ , then the total energy released by each burst is smaller by a factor  $\Delta\Omega/4\pi$  than the isotropic energy, and the GRB rate is larger by the same factor.

Due to present technical limitations of the experiments, afterglow radiation is observed in most cases only on time scale  $\gg 10$  s. At this stage, radiation is produced by the external shock driven into the surrounding gas, and afterglow observations therefore do not provide direct constraints on plasma parameters at the internal and reverse shocks, where protons are accelerated to ultra-high energy. In one case, however, that of GRB 990123, optical emission has been detected on  $\sim 10$  s time scale [2]. The most natural explanation of the observed optical radiation is synchrotron emission from electrons accelerated to high energy in the reverse shocks driven into fireball ejecta at the onset of interaction with the surrounding medium [73,89], as explained in §2.7. This observation provides therefore direct constraints on the fireball ejecta plasma. First, it provides strong support for one of the underlying assumptions of the dissipative fireball scenario described in §2.2, that the energy is carried from the underlying source in the form of proton kinetic energy. This is due to the fact that the observed radiation is well accounted for in a model where a shock propagates into fireball plasma composed of protons and electrons (rather than, e.g., pair plasma). Second, comparison of the observed flux with model predictions, Eqs. (17) and (18), implies  $\xi_e \sim \xi_B \sim 10^{-1}$ .

Afterglow observations imply that a significant fraction of the energy initially carried by the fireball is converted into  $\gamma$ -rays, i.e. that the observed  $\gamma$ -ray energy provides a rough estimate of the total fireball energy. This has been demonstrated for one case, that of GRB970508, by a comparison of the total fireball energy derived from long term radio observations with the energy emitted in  $\gamma$ -rays [114,34], and for a large number of bursts by a comparison of observed  $\gamma$ -ray energy with the total fireball energy estimate based on X-ray afterglow data [35]. In the context of the fireball model described in §2, the inferred high radiative efficiency implies that a significant fraction of the wind kinetic energy must be

converted to internal energy in internal shocks, and that electrons must carry a significant fraction of the internal energy, i.e. that  $\xi_e$  should be close to unity. We have already shown, see §2.6, that  $\xi_e$  values not far below unity are required to account for the observed  $\gamma$ -ray emission. Conversion in internal shocks of a large fraction of fireball kinetic energy to internal energy is possibly provided the variance in the Lorentz factors of fireball shells is large [44].

In accordance with the implications of afterglow observations, we assume in the discussion below of UHECR and neutrino production in GRB fireballs, that the fraction of fireball energy converted to internal energy carried by electrons, and hence to  $\gamma$ -rays, is large. For discussion of UHECR production under the assumption that only a negligible fraction,  $\sim m_e/m_p$ , of the fireball energy is converted to radiation see ref. [98].

## 4 UHECRs from GRB fireballs

### 4.1 Fermi acceleration in GRBs

In the fireball model, the observed radiation is produced, both during the GRB and the afterglow, by synchrotron emission of shock accelerated electrons. In the region where electrons are accelerated, protons are also expected to be shock accelerated. This is similar to what is thought to occur in supernovae remnant shocks, where synchrotron radiation of accelerated electrons is the likely source of non-thermal X-rays (recent ASCA observations give evidence for acceleration of electrons in the remnant of SN1006 to  $10^{14}$ eV [56]), and where shock acceleration of protons is believed to produce cosmic rays with energy extending to  $\sim 10^{15}$ eV (see, e.g., [14] for review). Thus, it is likely that protons, as well as electrons, are accelerated to high energy within GRB fireballs. Let us consider the constraints that should be satisfied by the fireball parameters in order to allow acceleration of protons to  $\sim 10^{20}$  eV.

We consider proton Fermi acceleration in fireball internal shocks, which take place as the fireball expands over a range of radii,  $r \sim \Gamma^2 r_0$  to  $r \sim \Gamma^2 cT_{\text{GRB}}$ , and at the reverse shocks driven into fireball ejecta due to interaction with surrounding medium at  $r \sim \Gamma^2 cT \sim \Gamma^2 cT_{\text{GRB}}$  (see §2.2, §2.4). Both internal and reverse shocks are, in the wind rest-frame, mildly relativistic, i.e. characterized by Lorentz factors  $\Gamma_i - 1 \sim 1$ . Moreover, since reverse shocks do not cause strong deceleration of fireball plasma, see §2.4, the expansion Lorentz factor  $\Gamma_{\text{tr}}$  of fireball plasma shocked by reverse shocks is similar to the fireball Lorentz factor  $\Gamma$  prior to interaction with the surrounding medium. Thus, plasma parameters, e.g. energy and number density, in the reverse shocks are similar to those obtained in internal shocks due to variability on time scale  $\Delta t \sim T$ . Results obtained below for internal shocks are therefore valid also for reverse shocks, provided  $\Delta t$  is replaced with  $T$ .

Since the shocks we are interested in are mildly relativistic, we expect results related to particle acceleration in sub-relativistic shocks (see [14] for review) to be valid for our scenario. The predicted energy distribution of accelerated

protons is therefore  $dn_p/d\epsilon_p \propto \epsilon_p^{-2}$  [4,10,16], similar to the predicted electron energy spectrum, which is consistent with the observed photon spectrum (see §2.6).

The most restrictive requirement, which rules out the possibility of accelerating particles to energy  $\sim 10^{20}$  eV in most astrophysical objects, is that the particle Larmor radius  $R_L$  should be smaller than the system size [52]. In our scenario we must apply a more stringent requirement, namely that  $R_L$  should be smaller than the largest scale  $l$  over which the magnetic field fluctuates, since otherwise Fermi acceleration may not be efficient. We may estimate  $l$  as follows. The comoving time, i.e. the time measured in the wind rest frame, is  $t = r/\Gamma c$ . Thus, regions separated by a comoving distance larger than  $r/\Gamma$  are causally disconnected, and the wind properties fluctuate over comoving length scales up to  $l \sim r/\Gamma$ . We must therefore require  $R_L < r/\Gamma$ . A somewhat more stringent requirement is related to the wind expansion. Due to expansion the internal energy is decreasing and therefore available for proton acceleration (as well as for  $\gamma$ -ray production) only over a comoving time  $t \sim r/\Gamma c$ . The typical Fermi acceleration time is  $t_a = fR_L/c\beta^2$  [52,14], where  $\beta c$  is the Alfvén velocity and  $f \sim 1$  [62]. In our scenario  $\beta \simeq 1$  leading to the requirement  $fR_L < r/\Gamma$ . This condition sets a lower limit to the required comoving magnetic field strength. Using the relations  $R_L = \epsilon'_p/eB = \epsilon_p/\Gamma eB$ , where  $\epsilon'_p = \epsilon_p/\Gamma$  is the proton energy measured in the fireball frame, and  $4\pi r^2 c \Gamma^2 B^2/8\pi = \xi_B L_\gamma/\xi_e$ , the constraint  $fR_L < r/\Gamma$  may be written as [104],

$$\xi_B/\xi_e > 0.02 f^2 \Gamma_{2.5}^2 \epsilon_{p,20}^2 L_{\gamma,52}^{-1}, \quad (21)$$

where  $\epsilon_p = 10^{20} \epsilon_{p,20}$  eV is the accelerated proton energy. Note, that this constraint is independent of  $r$ , the internal collision radius.

The accelerated proton energy is also limited by energy loss due to synchrotron radiation and interaction with fireball photons. As discussed in §6, the dominant energy loss process is synchrotron cooling. The condition that the synchrotron loss time,  $t_{sy} = (6\pi m_p^4 c^3 / \sigma_T m_e^2) \epsilon_p^{-1} B^{-2}$ , should be smaller than the acceleration time sets an upper limit to the magnetic field strength. Since the equipartition field decreases with radius,  $B_{e.p.} \propto r^{-2}$ , the upper limit on the magnetic field may be satisfied simultaneously with (21) provided that the internal collisions occur at large enough radius [104],

$$r > 10^{12} f^2 \Gamma_{2.5}^{-2} \epsilon_{p,20}^3 \text{ cm}. \quad (22)$$

Since collisions occur at radius  $r \approx \Gamma^2 c \Delta t$ , the condition (22) is equivalent to a lower limit on  $\Gamma$

$$\Gamma > 130 f^{1/2} \epsilon_{p,20}^{3/4} \Delta t_{-2}^{-1/4}. \quad (23)$$

From Eqs. (21) and (23), we infer that a dissipative ultra-relativistic wind, with luminosity and variability time implied by GRB observations, satisfies the constraints necessary to allow the acceleration of protons to energy  $> 10^{20}$  eV, provided that the wind bulk Lorentz factor is large enough,  $\Gamma > 100$ , and that the magnetic field is close to equipartition with electrons. The former constraint,  $\Gamma > 100$ , is remarkably similar to that inferred based on the  $\gamma$ -ray spectrum,

and  $\Gamma \sim 300$  is the “canonical” value assumed in the fireball model. The latter constraint, magnetic field close to equipartition, must be satisfied to account for both  $\gamma$ -ray emission (see §2.6) and afterglow observations (see §3).

Finally, two points should be clarified. First, it has recently been claimed that ultra-high energy protons would lose most of their energy adiabatically, i.e. due to expansion, before they escape the fireball [85]. This claim is based on the assumptions that internal shocks, and therefore proton acceleration, occur at  $r \sim \Gamma^2 r_0$  only, and that subsequently the fireball expands adiabatically. Under these assumptions, protons would lose most their energy by the time they escape. However, as emphasized both in this section and in §2.2, internal shocks are expected to occur over a wide range of radii, and in particular at  $r \sim \Gamma^2 cT$  during the transition to self-similar expansion. Thus, proton acceleration to ultra-high energy is expected to operate over a wide range of radii, from  $r \sim \Gamma^2 r_0$  up to  $r \sim \Gamma^2 cT$ , where ultra-high energy particles escape.

Second, it has recently been claimed in [40] that the conditions at the external shock driven by the fireball into the ambient gas are not likely to allow proton acceleration to ultra-high energy. Regardless of the validity of this claim, it is irrelevant for the acceleration in internal shocks, the scenario considered for UHECR production in GRBs in both [104] and [99]. Moreover, it is not at all clear that UHECRs can not be produced at the external shock, since the magnetic field may be amplified ahead of the shock by the streaming of high energy particles. For discussion of high energy proton production in the external shock and its possible implications see ref. [29].

## 4.2 UHECR flux and spectrum

Fly’s Eye [12,13] and AGASA [48,119,95] results confirm the flattening of the cosmic-ray spectrum at  $\sim 10^{19}$  eV, evidence for which existed in previous experiments with weaker statistics [102]. Fly’s Eye data is well fitted in the energy range  $10^{17.6}$  eV to  $10^{19.6}$  eV by a sum of two power laws: A steeper component, with differential number spectrum  $J \propto E^{-3.50}$ , dominating at lower energy, and a shallower component,  $J \propto E^{-2.61}$ , dominating at higher energy,  $E > 10^{19}$  eV. The flattening of the spectrum, combined with the lack of anisotropy and the evidence for a change in composition from heavy nuclei at low energy to light nuclei (protons) at high energy [102,12,13,38,27], suggest that a Galactic component of heavy nuclei,  $J \propto E^{-3.50}$ , dominates the cosmic-ray flux at low energy, while an extra-Galactic component of protons,  $J \propto E^{-2.61}$ , dominates the flux at high energy,  $> 10^{19}$  eV.

The GRB energy observed in  $\gamma$ -rays reflects the fireball energy in accelerated electrons. If accelerated electrons and protons carry similar energy, as indicated by afterglow observations [35] (see §3), then the GRB cosmic-ray production rate is [see Eq. (20)]

$$\epsilon_p^2(d\dot{n}_p/d\epsilon_p)_{z=0} \approx 10^{44} \text{ erg/Mpc}^3 \text{ yr.} \quad (24)$$

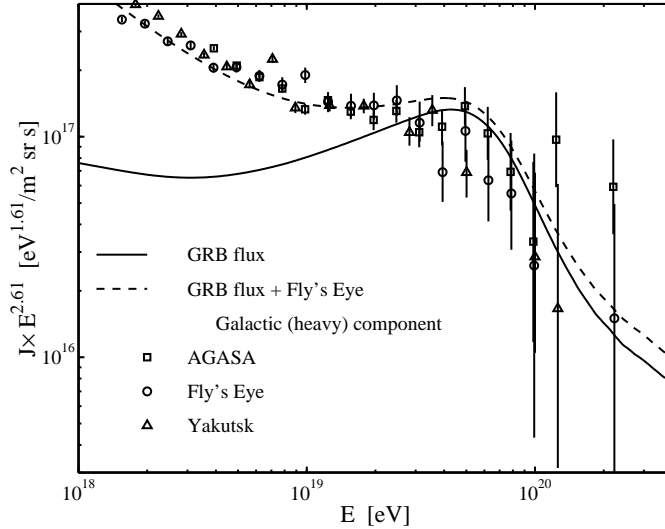


**Fig. 1.** The UHECR flux expected in a cosmological model, where high-energy protons are produced at a rate  $(\epsilon_p^2 \dot{n}_p / d\epsilon_p)_{z=0} = 0.8 \times 10^{44} \text{ erg/Mpc}^3 \text{ yr}$  as predicted by the GRB model [Eq. (24)], solid line, compared to the Fly's Eye [13], Yakutsk [30] and AGASA [49] data.  $1\sigma$  flux error bars are shown. The highest energy points are derived assuming the detected events represent a uniform flux over the energy range  $10^{20} \text{ eV} - 3 \times 10^{20} \text{ eV}$ . The dashed line is the sum of the GRB model flux and the Fly's Eye fit to the Galactic heavy nuclei component,  $J \propto \epsilon^{-3.5}$  [13] (with normalization increased by 25%).

In Fig. 1 we compare the UHECR spectrum, reported by the Fly's Eye [13], the Yakutsk [30], and the AGASA experiments [49], with that expected from a homogeneous cosmological distribution of sources, each generating a power law differential spectrum of high energy protons  $dn/d\epsilon_p \propto \epsilon_p^{-2}$ . The absolute flux measured at  $3 \times 10^{18} \text{ eV}$  differs between the various experiments, corresponding to a systematic  $\simeq 10\%$  ( $\simeq 20\%$ ) over-estimate of event energies in the AGASA (Yakutsk) experiment compared to the Fly's Eye experiment (see also [119]). In Fig. 1, the Yakutsk energy normalization is used. For the model calculation, a flat universe,  $\Omega = 0.3$ ,  $\Lambda = 0.7$  and  $H_0 = 65 \text{ km/Mpc s}$  were assumed. The calculation is similar to that described in [105]. The generation rate of cosmic-rays (per unit comoving volume) was assumed to evolve rapidly with redshift following the luminosity density evolution of QSOs [17], which is also similar to that describing the evolution of star formation rate [64,67]:  $\dot{n}_{CR}(z) \propto (1+z)^\alpha$  with  $\alpha \approx 3$  [51] at low redshift,  $z < 1.9$ ,  $\dot{n}_{CR}(z) = \text{Const.}$  for  $1.9 < z < 2.7$ , and an exponential decay at  $z > 2.7$  [90]. The cosmic-ray spectrum at energy  $> 10^{19} \text{ eV}$  is little affected by modifications of the cosmological parameters or of the redshift evolution of cosmic-ray generation rate. This is due to the fact that cosmic-rays at this energy originate from distances shorter than several hundred Mpc. The spectrum and flux at  $\epsilon_p > 10^{19} \text{ eV}$  is mainly determined by the present



( $z = 0$ ) generation rate and spectrum, which in the model shown in Fig. 1 is  $\epsilon_p^2(d\dot{n}_p/d\epsilon)_{z=0} = 0.8 \times 10^{44} \text{erg/Mpc}^3 \text{yr}$ .

The suppression of model flux above  $10^{19.7} \text{ eV}$  is due to energy loss of high energy protons in interaction with the microwave background, i.e. to the ‘‘GZK cutoff’’ [43,120]. The available data do not allow to determine the existence (or absence) of the ‘‘cutoff’’ with high confidence. The AGASA results show an excess (at a  $\sim 2.5\sigma$  confidence level) of events compared to model predictions above  $10^{20} \text{ eV}$ . This excess is not confirmed, however, by the other experiments. Moreover, since the  $10^{20} \text{ eV}$  flux is dominated by sources at distances  $< 100 \text{ Mpc}$ , over which the distribution of known astrophysical systems (e.g. galaxies, clusters of galaxies) is inhomogeneous, significant deviations from model predictions presented in Fig. 1 for a uniform source distribution are expected at this energy [105]. Clustering of cosmic-ray sources leads to a standard deviation,  $\sigma$ , in the expected number,  $N$ , of events above  $10^{20} \text{ eV}$ , given by  $\sigma/N = 0.9(d_0/10\text{Mpc})^{0.9}$  [7], where  $d_0$  is the unknown scale length of the source correlation function and  $d_0 \sim 10 \text{ Mpc}$  for field galaxies.

Thus, GRB fireballs would produce UHECR flux and spectrum consistent with that observed, provided the efficiency with which the wind kinetic energy is converted to  $\gamma$ -rays, and therefore to electron energy, is similar to the efficiency with which it is converted to proton energy, i.e. to UHECRs [104]. There is, however, one additional point which requires consideration [104]. The energy of the most energetic cosmic ray detected by the Fly’s Eye experiment is in excess of  $2 \times 10^{20} \text{ eV}$ , and that of the most energetic AGASA event is  $\sim 2 \times 10^{20} \text{ eV}$ . On a cosmological scale, the distance traveled by such energetic particles is small:  $< 100 \text{ Mpc}$  ( $50 \text{ Mpc}$ ) for the AGASA (Fly’s Eye) event (e.g., [1]). Thus, the detection of these events over a  $\sim 5 \text{ yr}$  period can be reconciled with the rate of nearby GRBs,  $\sim 1 \text{ per } 100 \text{ yr}$  to  $\sim 1 \text{ per } 1000 \text{ yr}$  out to  $100 \text{ Mpc}$ , only if there is a large dispersion,  $\geq 100 \text{ yr}$ , in the arrival time of protons produced in a single burst (This implies that if a direct correlation between high energy CR events and GRBs, as suggested in [75], is observed on a  $\sim 10 \text{ yr}$  time scale, it would be strong evidence *against* a cosmological GRB origin of UHECRs).

The required dispersion is likely to occur due to the combined effects of deflection by random magnetic fields and energy dispersion of the particles [104]. Consider a proton of energy  $\epsilon_p$  propagating through a magnetic field of strength  $B$  and correlation length  $\lambda$ . As it travels a distance  $\lambda$ , the proton is typically deflected by an angle  $\alpha \sim \lambda/R_L$ , where  $R_L = \epsilon_p/eB$  is the Larmor radius. The typical deflection angle for propagation over a distance  $D$  is  $\theta_s \approx (2D/9\lambda)^{1/2} \lambda/R_L$ . This deflection results in a time delay, compared to propagation along a straight line,

$$\tau(\epsilon_p, D) \approx \theta_s^2 D/4c \approx 10^7 \epsilon_{p,20}^{-2} D_{100}^2 \lambda_{\text{Mpc}} B_{-8}^2 \text{ yr}, \quad (25)$$

where  $D = 100 D_{100} \text{ Mpc}$ ,  $\lambda = 1 \lambda_{\text{Mpc}} \text{ Mpc}$  and  $B = 10^{-8} B_{-8} \text{ G}$ . Here, we have chosen numerical values corresponding to the current upper bound on the inter-galactic magnetic field,  $B \lambda^{1/2} \leq 10^{-8} \text{ G Mpc}^{1/2}$  [59,58]. The upper bound on the (systematic increase with redshift of the) Faraday rotation measure of distant,  $z \leq 2.5$ , radio sources,  $RM < 5 \text{ rad/m}^2$ , implies an upper bound  $B \leq$

$10^{-11}(h/0.75)(\Omega_b h^2)^{-1}$  G on an inter-galactic field coherent over cosmological scales [58]. Here,  $h$  is the Hubble constant in units of 100km/sMpc and  $\Omega_b$  is the baryon density in units of the closure density. For a magnetic field coherent on scales  $\sim \lambda$ , this implies  $B\lambda^{1/2} \leq 10^{-8}(h/0.65)^{1/2}(\Omega_b h^2/0.04)^{-1}$  G Mpc<sup>1/2</sup>.

The random energy loss UHECRs suffer as they propagate, owing to the production of pions, implies that at any distance from the observer there is some finite spread in the energies of UHECRs that are observed with a given fixed energy. For protons with energies  $> 10^{20}$ eV the fractional RMS energy spread is of order unity over propagation distances in the range 10 – 100Mpc (e.g. [1]). Since the time delay is sensitive to the particle energy, this implies that the spread in arrival time of UHECRs with given observed energy is comparable to the average time delay at that energy  $\tau(\epsilon_p, D)$  (This result has been confirmed by numerical calculations in [112]). Thus, the required time spread,  $\tau > 100$  yr, is consistent with the upper bound,  $\tau < 10^7$  yr, implied by the present upper bound to the inter-galactic magnetic field.

## 5 GRB model predictions for UHECR experiments

### 5.1 The Number and Spectra of Bright Sources

The initial proton energy, necessary to have an observed energy  $\epsilon_p$ , increases with source distance due to propagation energy losses. The rapid increase of the initial energy after it exceeds, due to electron-positron production, the threshold for pion production effectively introduces a cutoff distance,  $D_c(\epsilon_p)$ , beyond which sources do not contribute to the flux above  $\epsilon_p$ . The function  $D_c(\epsilon_p)$  is shown in Fig. 3 (adapted from [76]). Since  $D_c(\epsilon_p)$  is a decreasing function of  $\epsilon_p$ , for a given number density of sources there is a critical energy  $\epsilon_c$ , above which only one source (on average) contributes to the flux. In the GRB model  $\epsilon_c$  depends on the product of the burst rate  $R_{GRB}$  and the time delay. The number of sources contributing, on average, to the flux at energy  $\epsilon_p$  is [76]

$$N(\epsilon_p) = \frac{4\pi}{5} R_{GRB} D_c(\epsilon_p)^3 \tau[\epsilon_p, D_c(\epsilon_p)] \quad , \quad (26)$$

and the average intensity resulting from all sources is

$$J(\epsilon_p) = \frac{1}{4\pi} R_{GRB} \frac{dn_p}{d\epsilon_p} D_c(\epsilon_p) \quad , \quad (27)$$

where  $dn_p/d\epsilon_p$  is the number per unit energy of protons produced on average by a single burst (this is the formal definition of  $D_c(\epsilon_p)$ ). The critical energy  $\epsilon_c$  is given by

$$\frac{4\pi}{5} R_{GRB} D_c(\epsilon_c)^3 \tau[\epsilon_c, D_c(\epsilon_c)] = 1 \quad . \quad (28)$$

$\epsilon_c$ , the energy beyond which a single source contributes on average to the flux, depends on the unknown properties of the inter-galactic magnetic field,  $\tau \propto B^2 \lambda$ . However, the rapid decrease of  $D_c(\epsilon_p)$  with energy near  $10^{20}$ eV implies

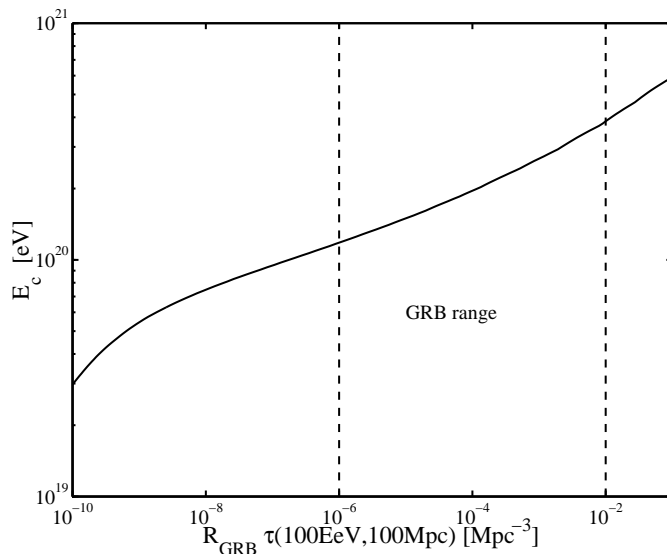


**Fig. 2.**  $\epsilon_c$ , the energy beyond which a single GRB contributes on average to the UHECR flux, as a function of the product of GRB rate,  $R_{GRB} \approx 1/\text{Gpc}^3$ , and the time delay of a  $10^{20}$  eV proton originating at 100 Mpc distance. The time delay depends on the unknown inter-galactic field,  $\tau \propto B^2\lambda$ . Dashed lines show the allowed range of  $B^2\lambda$ : The lower limit is set by the requirement that at least a few GRB sources be present at  $D < 100$  Mpc, and the upper limit by the Faraday rotation bound  $B\lambda^{1/2} \leq 10^{-8} \text{G Mpc}^{1/2}$  [58], see Eq. (25) and the discussion the follows it.

that  $\epsilon_c$  is only weakly dependent on the value of  $B^2\lambda$ , as shown in Fig. 2. In The GRB model, the product  $R_{GRB}\tau(D = 100\text{Mpc}, \epsilon_p = 10^{20}\text{eV})$  is approximately limited to the range  $10^{-6} \text{Mpc}^{-3}$  to  $10^{-2} \text{Mpc}^{-3}$  [The lower limit is set by the requirement that at least a few GRB sources be present at  $D < 100$  Mpc, and the upper limit by the Faraday rotation bound  $B\lambda^{1/2} \leq 10^{-8} \text{G Mpc}^{1/2}$  [58], see Eq. (25), and  $R_{GRB} \leq 1/\text{Gpc}^3\text{yr}$ ]. The corresponding range of values of  $\epsilon_c$  is  $10^{20}\text{eV} \leq \epsilon_c < 4 \times 10^{20}\text{eV}$ .

Fig. 3 presents the flux obtained in one realization of a Monte-Carlo simulation described by Miralda-Escudé & Waxman [76] of the total number of UHECRs received from GRBs at some fixed time. For each realization the positions (distances from Earth) and times at which cosmological GRBs occurred were randomly drawn, assuming an intrinsic proton generation spectrum  $dn_p/d\epsilon_p \propto \epsilon_p^{-2}$ , and  $\epsilon_c = 1.4 \times 10^{20}\text{eV}$ . Most of the realizations gave an overall spectrum similar to that obtained in the realization of Fig. 3 when the brightest source of this realization (dominating at  $10^{20}\text{eV}$ ) is not included. At  $\epsilon_p < \epsilon_c$ , the number of sources contributing to the flux is very large, and the overall UHECR flux received at any given time is near the average (the average flux is that obtained when the UHECR emissivity is spatially uniform and time independent). At  $\epsilon_p > \epsilon_c$ , the flux will generally be much lower than the average, because there will be no

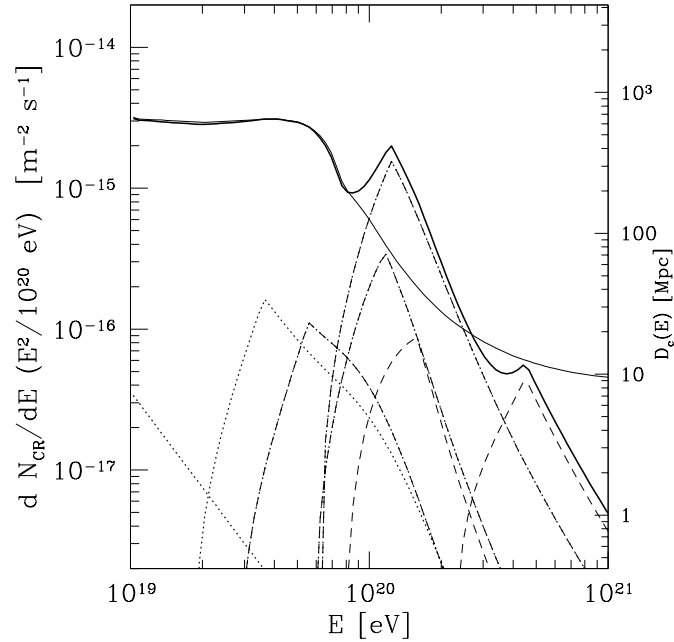


**Fig. 3.** Results of a Monte-Carlo realization of the bursting sources model, with  $\epsilon_c = 1.4 \times 10^{20}$  eV: Thick solid line- overall spectrum in the realization; Thin solid line- average spectrum, this curve also gives  $D_c(\epsilon_p)$ ; Dotted lines- spectra of brightest sources at different energies.

burst within a distance  $D_c(\epsilon_p)$  having taken place sufficiently recently. There is, however, a significant probability to observe one source with a flux higher than the average. A source similar to the brightest one in Fig. 3 appears  $\sim 5\%$  of the time.

At any fixed time a given burst is observed in UHECRs only over a narrow range of energy, because if a burst is currently observed at some energy  $\epsilon_p$  then UHECRs of much lower energy from this burst have not yet arrived, while higher energy UHECRs reached us mostly in the past. As mentioned above, for energies above the pion production threshold,  $\epsilon_p \sim 5 \times 10^{19}$  eV, the dispersion in arrival times of UHECRs with fixed observed energy is comparable to the average delay at that energy. This implies that the spectral width  $\Delta\epsilon_p$  of the source at a given time is of order the average observed energy,  $\Delta\epsilon_p \sim \epsilon_p$ . Thus, bursting UHECR sources should have narrowly peaked energy spectra, and the brightest sources should be different at different energies. For steady state sources, on the other hand, the brightest source at high energies should also be the brightest one at low energies, its fractional contribution to the overall flux decreasing to low energy only as  $D_c(\epsilon_p)^{-1}$ . A detailed numerical analysis of the time dependent energy spectrum of bursting sources is given in [92,63].

## 5.2 Spectra of Sources at $\epsilon_p < 4 \times 10^{19}$ eV

The detection of UHECRs above  $10^{20}$  eV imply that the brightest sources must lie at distances smaller than 100Mpc. UHECRs with  $\epsilon_p \leq 4 \times 10^{19}$  eV from such bright sources will suffer energy loss only by pair production, because at  $\epsilon_p < 5 \times 10^{19}$  eV the mean-free-path for pion production interaction (in which the fractional energy loss is  $\sim 10\%$ ) is larger than 1Gpc. Furthermore, the energy loss due to pair production over 100Mpc propagation is only  $\sim 5\%$ .

In the case where the typical displacement of the UHECRs due to deflections by inter-galactic magnetic fields is much smaller than the correlation length,  $\lambda \gg D\theta_s(D, \epsilon_p) \simeq D(D/\lambda)^{1/2}\lambda/R_L$ , all the UHECRs that arrive at the observer are essentially deflected by the same magnetic field structures, and the absence of random energy loss during propagation implies that all rays with a fixed observed energy would reach the observer with exactly the same direction and time delay. At a fixed time, therefore, the source would appear mono-energetic and point-like. In reality, energy loss due to pair production results in a finite but small spectral and angular width,  $\Delta\epsilon_p/\epsilon_p \sim \delta\theta/\theta_s \leq 1\%$  [115].

In the case where the typical displacement of the UHECRs is much larger than the correlation length,  $\lambda \ll D\theta_s(D, \epsilon_p)$ , the deflection of different UHECRs arriving at the observer are essentially independent. Even in the absence of any energy loss there are many paths from the source to the observer for UHECRs of fixed energy  $\epsilon_p$  that are emitted from the source at an angle  $\theta \leq \theta_s$  relative to the source-observer line of sight. Along each of the paths, UHECRs are deflected by independent magnetic field structures. Thus, the source angular size would be of order  $\theta_s$  and the spread in arrival times would be comparable to the characteristic delay  $\tau$ , leading to  $\Delta\epsilon_p/\epsilon_p \sim 1$  even when there are no random energy losses. The observed spectral shape of a nearby ( $D < 100$ Mpc) bursting source of UHECRs at  $\epsilon_p < 4 \times 10^{19}$  eV was derived for the case  $\lambda \ll D\theta_s(D, \epsilon_p)$  in [115], and is given by

$$\frac{dN}{d\epsilon_p} \propto \sum_{n=1}^{\infty} (-1)^{n+1} n^2 \exp\left[-\frac{2n^2\pi^2\epsilon^2}{\epsilon_0^2(t, D)}\right], \quad (29)$$

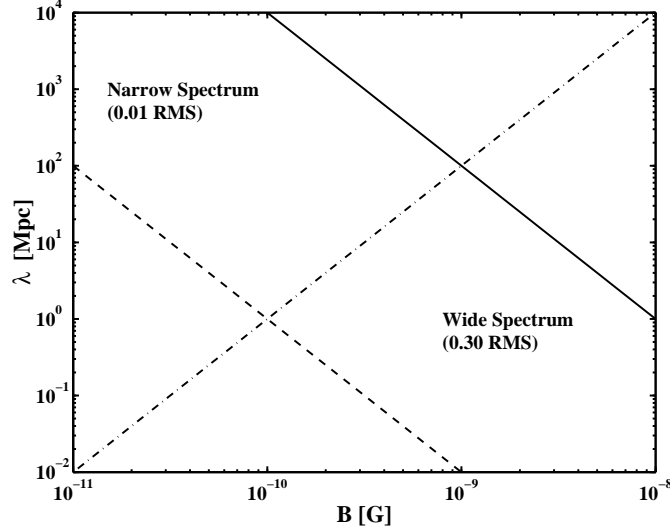
where  $\epsilon_0(t, D) = De(2B^2\lambda/3ct)^{1/2}$ . For this spectrum, the ratio of the RMS UHECR energy spread to the average energy is 30%

Fig. 4 shows the line  $\theta_s D = \lambda$  in the  $B - \lambda$  plane, for a source at a distance  $D = 30$ Mpc observed at energy  $\epsilon_p \simeq 10^{19}$  eV. Since the  $\theta_s D = \lambda$  line divides the allowed region in the plane at  $\lambda \sim 1$ Mpc, measuring the spectral width of bright sources would allow to determine if the field correlation length is much larger, much smaller, or comparable to 1Mpc.

## 6 High energy Neutrinos

### 6.1 Internal shock (GRB) neutrinos

**Neutrinos at energies  $\sim 10^{14}$  eV.** Protons accelerated in the fireball to high energy lose energy through photo-meson interaction with fireball photons.



**Fig. 4.** The line  $\theta_s D = \lambda$  for a source at 30Mpc distance observed at energy  $\epsilon_p \simeq 10^{19}$ eV (dot-dash line), shown with the Faraday rotation upper limit  $B\lambda^{1/2} \leq 10^{-8}$ G Mpc $^{1/2}$  (solid line), and with the lower limit  $B\lambda^{1/2} \geq 10^{-10}$ G Mpc $^{1/2}$  required in the GRB model [see Eq. (25)].

The decay of charged pions produced in this interaction,  $\pi^+ \rightarrow \mu^+ + \nu_\mu \rightarrow e^+ + \nu_e + \bar{\nu}_\mu + \nu_\mu$ , results in the production of high energy neutrinos. The key relation is between the observed photon energy,  $\epsilon_\gamma$ , and the accelerated proton's energy,  $\epsilon_p$ , at the threshold of the  $\Delta$ -resonance. In the observer frame,

$$\epsilon_\gamma \epsilon_p = 0.2 \text{ GeV}^2 \Gamma^2. \quad (30)$$

For  $\Gamma \approx 300$  and  $\epsilon_\gamma = 1$  MeV, we see that characteristic proton energies  $\sim 10^{16}$  eV are required to produce pions. Since neutrinos produced by pion decay typically carry 5% of the proton energy (see below), production of  $\sim 10^{14}$  eV neutrinos is expected [109,110].

The fractional energy loss rate of a proton with energy  $\epsilon'_p = \epsilon_p/\Gamma$  measured in the wind rest frame due to pion production is

$$\begin{aligned} t_\pi^{-1}(\epsilon'_p) &\equiv -\frac{1}{\epsilon'_p} \frac{d\epsilon'_p}{dt} \\ &= \frac{1}{2\gamma_p^2} c \int_{\epsilon_0}^{\infty} d\epsilon \sigma_\pi(\epsilon) \xi(\epsilon) \epsilon \int_{\epsilon/2\Gamma_p}^{\infty} dx x^{-2} \frac{dn_\gamma}{d\epsilon_\gamma}(\epsilon_\gamma = x), \end{aligned} \quad (31)$$

where  $\gamma_p = \epsilon'_p/m_p c^2$ ,  $\sigma_\pi(\epsilon)$  is the cross section for pion production for a photon with energy  $\epsilon$  in the proton rest frame,  $\xi(\epsilon)$  is the average fraction of energy lost to the pion,  $\epsilon_0 = 0.15$ GeV is the threshold energy, and  $dn_\gamma/d\epsilon_\gamma$  is the photon density per unit photon energy in the wind rest frame. In deriving Eq. (31) we

have assumed that the photon distribution in the wind rest frame is isotropic. The GRB photon spectrum is well fitted in the BATSE detector range, 20 keV to 2 MeV, by a combination of two power-laws,  $dn_\gamma/d\epsilon_\gamma \propto \epsilon_\gamma^{-\beta}$ , with  $\beta \simeq 1$  at  $\epsilon_\gamma < \epsilon_{\gamma b}$ ,  $\beta \simeq 2$  at  $\epsilon_\gamma > \epsilon_{\gamma b}$  and  $\epsilon_{\gamma b} \sim 1\text{MeV}$  [8]. Thus, the second integral in (31) may be approximated by

$$\int_\epsilon^\infty dx x^{-2} \frac{dn_\gamma}{d\epsilon_\gamma}(\epsilon_\gamma = x) \simeq \frac{1}{1+\beta} \frac{U_\gamma}{2\epsilon_{\gamma b}^3} \left( \frac{\epsilon}{\epsilon_{\gamma b}} \right)^{-(1+\beta)}, \quad (32)$$

where  $U_\gamma$  is the photon energy density (in the range corresponding to the observed BATSE range) in the wind rest-frame,  $\beta = 1$  for  $\epsilon < \epsilon'_{\gamma b}$  and  $\beta = 2$  for  $\epsilon > \epsilon'_{\gamma b}$ .  $\epsilon'_{\gamma b}$  is the break energy measured in the wind frame,  $\epsilon'_{\gamma b} = \epsilon_{\gamma b}/\Gamma$ . The main contribution to the first integral in (31) is from photon energies  $\epsilon \sim \epsilon_{\text{peak}} = 0.3\text{GeV}$ , where the cross section peaks due to the  $\Delta$  resonance. Approximating the integral by the contribution from the resonance we obtain

$$t_\pi^{-1}(\epsilon'_p) \simeq \frac{U_\gamma}{2\epsilon'_{\gamma b}} c\sigma_{\text{peak}}\xi_{\text{peak}} \frac{\Delta\epsilon}{\epsilon_{\text{peak}}} \min(1, 2\gamma_p\epsilon'_{\gamma b}/\epsilon_{\text{peak}}). \quad (33)$$

Here,  $\sigma_{\text{peak}} \simeq 5 \times 10^{-28}\text{cm}^2$  and  $\xi_{\text{peak}} \simeq 0.2$  are the values of  $\sigma$  and  $\xi$  at  $\epsilon = \epsilon_{\text{peak}}$ , and  $\Delta\epsilon \simeq 0.2\text{GeV}$  is the peak width.

The energy loss of protons due to pion production is small during the acceleration process. Once accelerated, the time available for proton energy loss by pion production is comparable to the wind expansion time as measured in the wind rest frame,  $t_{\text{co}} \sim r/\Gamma c$ . Thus, the fraction of energy lost by protons to pions is  $f_\pi \simeq r/\Gamma ct_\pi$ . The energy density in the BATSE range,  $U_\gamma$ , is related to the luminosity  $L_\gamma$  by  $L_\gamma = 4\pi r^2 \Gamma^2 c U_\gamma$ . Using this relation in (33), and  $r = 2\Gamma^2 c \Delta t$ ,  $f_\pi$  is given by [109]

$$f_\pi(\epsilon_p) \approx 0.1 \frac{L_{\gamma,52}}{\epsilon_{\gamma b, \text{MeV}} \Gamma_{2.5}^4 \Delta t_{-2}} \times \begin{cases} 1, & \text{if } \epsilon_p > \epsilon_{pb}; \\ \epsilon_p/\epsilon_{pb}, & \text{otherwise.} \end{cases} \quad (34)$$

The proton break energy is

$$\epsilon_{pb} \approx 10^{16} \Gamma_{2.5}^2 (\epsilon_{\gamma b, \text{MeV}})^{-1} \text{eV}. \quad (35)$$

The value of  $f_\pi$ , Eq. (34), is strongly dependent on  $\Gamma$ . It has recently been pointed out [47] that if the Lorentz factor  $\Gamma$  varies significantly between bursts, with burst to burst variations  $\Delta\Gamma/\Gamma \sim 1$ , then the resulting neutrino flux will be dominated by a few neutrino bright bursts, and may significantly exceed the flux implied by Eq. (34), derived for typical burst parameters. This may strongly enhance the detectability of GRB neutrinos by planned neutrino telescopes [3]. However, as explained in §2.6, the Lorentz factors of fireballs producing observed GRBs can not differ significantly from the minimum value allowed by Eq. (5),  $\Gamma \simeq 250$ , for which the fireball pair production optical depth, Eq. (4), is  $\approx 1$  for  $\epsilon_\gamma = 100 \text{ MeV}$ : Lower Lorentz factors lead to optically thick fireballs, while higher Lorentz factors lead to low luminosity X-ray bursts (which may have

already been identified). Thus, for Lorentz factors consistent with observed GRB spectra, for which  $\tau_{\gamma\gamma}(\epsilon_\gamma = 100\text{MeV}) \approx 1$ , we find

$$f_\pi(\epsilon_p) \approx 0.2 \frac{L_{\gamma,52}^{1/3}}{\epsilon_{\gamma b, \text{MeV}} \Delta t_{-2}^{1/3}} \times \begin{cases} 1, & \text{if } \epsilon_p > \epsilon_{pb}; \\ \epsilon_p/\epsilon_{pb}, & \text{otherwise.} \end{cases} \quad (36)$$

A detailed analysis, using Monte-Carlo simulations of the internal shock model, confirms that for fireball parameter range consistent with observed GRB characteristics,  $f_\pi$  at  $\epsilon_p > \epsilon_{pb}$  is limited to the range of  $\sim 10\%$  to  $30\%$  [45].

Thus, for parameters typical of a GRB producing wind, a significant fraction of the energy of protons accelerated to energies larger than the break energy,  $\sim 10^{16}\text{eV}$ , would be lost to pion production. Roughly half of the energy lost by protons goes into  $\pi^0$ 's and the other half to  $\pi^\pm$ 's. Neutrinos are produced by the decay of  $\pi^\pm$ 's,  $\pi^\pm \rightarrow \mu^\pm + \nu_\mu \rightarrow e^\pm + \nu_e + \bar{\nu}_\mu + \nu_\mu$  [the large optical depth for high energy  $\gamma$ 's from  $\pi^0$  decay, Eq. (4), would not allow these photons to escape the wind]. The mean pion energy is 20% of the energy of the proton producing the pion. This energy is roughly evenly distributed between the  $\pi^\pm$  decay products. Thus, approximately half the energy lost by protons of energy  $\epsilon_p$  is converted to neutrinos with energy  $\sim 0.05\epsilon_p$ . Eq. (34) then implies that the spectrum of neutrinos above  $\epsilon_{\nu b} = 0.05\epsilon_{pb}$  follows the proton spectrum, and is harder (by one power of the energy) at lower energy.

If GRBs are the sources of UHECRS, then using Eq. (24) the expected GRB neutrino flux is [110]

$$\begin{aligned} \epsilon_\nu^2 \Phi_{\nu_\mu} &\approx \epsilon_\nu^2 \Phi_{\bar{\nu}_\mu} \approx \epsilon_\nu^2 \Phi_{\nu_e} \approx \frac{c}{4\pi} \frac{f_\pi}{8} \epsilon_p^2 (d\dot{n}_p/d\epsilon_p) t_H \\ &\approx 1.5 \times 10^{-9} \frac{f_\pi(\epsilon_{pb})}{0.2} \min\{1, \epsilon_\nu/\epsilon_{\nu b}\} \text{GeV cm}^{-2} \text{s}^{-1} \text{sr}^{-1}, \end{aligned} \quad (37)$$

where  $t_H \approx 10^{10}$  yr is the Hubble time. The factor of  $1/8$  is due to the fact that charged pions and neutral pions are produced with roughly equal probabilities (and each neutrino carries  $\sim 1/4$  of the pion energy).

The GRB neutrino flux can also be estimated directly from the observed gamma-ray fluence. The BATSE detectors measure the GRB fluence  $F_\gamma$  over two decades of photon energy,  $\sim 0.02\text{MeV}$  to  $\sim 2\text{MeV}$ , corresponding to a decade of radiating electron energy (the electron synchrotron frequency is proportional to the square of the electron Lorentz factor). If electrons carry a fraction  $\xi_e$  of the energy carried by protons, then the muon neutrino fluence of a single burst is  $\epsilon_\nu^2 dN_\nu/d\epsilon_\nu \approx 0.25(f_\pi/\xi_e)F_\gamma/\ln(10)$ . The average neutrino flux per unit time and solid angle is obtained by multiplying the single burst fluence with the GRB rate per solid angle,  $\approx 10^3$  bursts per year over  $4\pi$  sr. Using the average burst fluence  $F_\gamma = 10^{-5}\text{erg/cm}^2$ , we obtain a muon neutrino flux  $\epsilon_\nu^2 \Phi_\nu \approx 3 \times 10^{-9}(f_\pi/\xi_e)\text{GeV/cm}^2\text{s sr}$ . Thus, the neutrino flux estimated directly from the gamma-ray fluence agrees with the estimate (37) based on the cosmic-ray production rate.



**Neutrinos at energy  $> 10^{16}$  eV.** The neutrino spectrum (37) is modified at high energy, where neutrinos are produced by the decay of muons and pions whose life time  $\tau_{\mu,\pi}$  exceeds the characteristic time for energy loss due to adiabatic expansion and synchrotron emission [109,86,110]. The synchrotron loss time is determined by the energy density of the magnetic field in the wind rest frame. For the characteristic parameters of a GRB wind, the muon energy for which the adiabatic energy loss time equals the muon life time,  $\epsilon_\mu^a$ , is comparable to the energy  $\epsilon_\mu^s$  at which the life time equals the synchrotron loss time,  $\tau_\mu^s$ . For pions,  $\epsilon_\pi^a > \epsilon_\pi^s$ . This, and the fact that the adiabatic loss time is independent of energy and the synchrotron loss time is inversely proportional to energy, imply that synchrotron losses are the dominant effect suppressing the flux at high energy. The energy above which synchrotron losses suppress the neutrino flux is

$$\frac{\epsilon_{\nu_\mu(\bar{\nu}_\mu, \nu_e)}^s}{\epsilon_{\nu b}} \approx \left( \frac{\xi_B}{\xi_e} L_{\gamma,52} \right)^{-1/2} \Gamma_{2.5}^2 \Delta t_{-2} \epsilon_{\gamma b, \text{MeV}} \times \begin{cases} 10, & \text{for } \bar{\nu}_\mu, \nu_e; \\ 100, & \text{for } \nu_\mu. \end{cases} \quad (38)$$

The efficiency of neutrino production in internal collisions decreases with  $\Delta t$ ,  $f_\pi \propto \Delta t^{-1}$  [see Eq. (34)], since the radiation energy density is lower at larger collision radii. However, at larger radii synchrotron losses cut off the spectrum at higher energy,  $\epsilon^s(\Delta t) \propto \Delta t$  [see Eq. (38)]. Collisions at large radii therefore result in extension of the neutrino spectrum of Eq. (37) to higher energy, beyond the cutoff energy Eq. (38),

$$\epsilon_\nu^2 \Phi_\nu \propto \epsilon_\nu^{-1}, \quad \epsilon_\nu > \epsilon_\nu^s. \quad (39)$$

**Comparison with other authors.** We note, that the results presented above were derived using the  $\Delta$ -approximation, i.e. assuming that photo-meson interactions are dominated by the contribution of the  $\Delta$ -resonance. It has recently been shown [77], that for photon spectra harder than  $dn_\gamma/d\epsilon_\gamma \propto \epsilon_\gamma^{-2}$ , the contribution of non-resonant interactions may be important. Since in order to interact with the hard part of the photon spectrum,  $\epsilon_\gamma < \epsilon_{\gamma b}$ , the proton energy must exceed the energy at which neutrinos of energy  $\epsilon_{\nu b}$  are produced, significant modification of the  $\Delta$ -approximation results is expected only for  $\epsilon_\nu \gg \epsilon_{\nu b}$ , where the neutrino flux is strongly suppressed by synchrotron losses.

The neutrino flux from GRBs is small above  $10^{19}$ eV, and a neutrino flux comparable to the  $\gamma$ -ray flux is expected only below  $\sim 10^{17}$ eV, in agreement with the results of ref. [86]. Our result is not in agreement, however, with that of ref. [101], where a much higher flux at  $\sim 10^{19}$ eV is obtained based on the equations of ref. [109], which are the same equations as used here<sup>1</sup>.

---

<sup>1</sup> The parameters chosen in [101] are  $L_\gamma = 10^{50}$ erg/s,  $\Delta t = 10$ s, and  $\Gamma = 100$ . Using equation (4) of ref. [109], which is the same as Eq. (34) of the present paper, we obtain for these parameters  $f_\pi = 1.6 \times 10^{-4}$ , while the author of [101] obtains, using the same equation,  $f_\pi = 0.03$ .

## 6.2 Reverse shock (afterglow) neutrinos, $\sim 10^{18}$ eV

Let us now consider neutrino emission from photo-meson interactions of protons accelerated to high energies in the reverse shocks driven into the fireball ejecta at the initial stage of interaction of the fireball with its surrounding gas, which occurs on time scale  $T \sim 10$  s, comparable to the duration of the GRB itself (see §2.4). Optical–UV photons are radiated by electrons accelerated in shocks propagating backward into the ejecta (see §2.7), and may interact with accelerated protons. The interaction of these low energy, 10 eV–1 keV, photons and high energy protons produces a burst of duration  $\sim T$  of ultra-high energy,  $10^{17}$ – $10^{19}$  eV, neutrinos [as indicated by Eq. (30)] via photo-meson interactions [111].

Afterglows have been detected in several cases; reverse shock emission has only been identified for GRB 990123 [2]. Both the detections and the non-detections are consistent with shocks occurring with typical model parameters [113,89,73], suggesting that reverse shock emission may be common. The predicted neutrino emission depends, however, upon parameters of the surrounding medium that can only be estimated once more observations of the prompt optical afterglow emission are available. We first consider the case where the density of gas surrounding the fireball is  $n \sim 1\text{cm}^{-3}$ , a value typical to the inter-stellar medium and consistent with GRB 990123 observations.

The photon density in Eq. (31) is related to the observed specific luminosity by  $dn_\gamma/d\epsilon_\gamma(x) = L_\epsilon(\Gamma x)/(4\pi r^2 c \Gamma x)$ . For proton Lorentz factor  $\epsilon_0/2\epsilon'_{\gamma c} \ll \gamma_p < \epsilon_0/2\epsilon'_{\gamma m}$ , where primed energies denote rest frame energies (e.g.  $\epsilon'_{\gamma m} = \epsilon_{\gamma m}/\Gamma_{\text{tr}}$ ), photo-meson production is dominated by interaction with photons in the energy range  $\epsilon_{\gamma m} < \epsilon_\gamma \ll \epsilon_{\gamma c}$ , where  $L_\epsilon \propto \epsilon_\gamma^{-1/2}$  (see §2.7). For this photon spectrum, the contribution to the first integral of Eq. (31) from photons at the  $\Delta$ -resonance is comparable to that of photons of higher energy, and we obtain

$$t_\pi^{-1}(\epsilon'_p) \simeq \frac{2^{5/2}}{2.5} \frac{L_m}{4\pi r^2 \Gamma_{\text{tr}}} \left( \frac{\epsilon_{\text{peak}}}{\gamma_p \epsilon'_{\gamma m}} \right)^{-1/2} \frac{\sigma_{\text{peak}} \xi_{\text{peak}} \Delta \epsilon}{\epsilon_{\text{peak}}}. \quad (40)$$

$\Gamma_{\text{tr}}$  is the expansion Lorentz factor of plasma shocked by the reverse shocks, given by Eq. (14). The time available for proton energy loss by pion production is comparable to the expansion time as measured in the wind rest frame,  $\sim r/\Gamma_{\text{tr}}c$ . Thus, the fraction of energy lost by protons to pions is

$$f_\pi(\epsilon_p) \approx 0.1 \left( \frac{L_m}{10^{61}\text{s}^{-1}} \right) \left( \frac{\Gamma_{\text{tr}}}{250} \right)^{-5} T_1^{-1} \times (\epsilon_{\gamma m, \text{eV}} \epsilon_{p,20})^{1/2}. \quad (41)$$

Eq. (41) is valid for protons in the energy range

$$4 \times 10^{18} \left( \frac{\Gamma_{\text{tr}}}{250} \right)^2 (\epsilon_{\gamma c, \text{keV}})^{-1} \text{eV} < \epsilon_p < 4 \times 10^{21} \left( \frac{\Gamma_{\text{tr}}}{250} \right)^2 (\epsilon_{\gamma m, \text{eV}})^{-1} \text{eV}. \quad (42)$$

Such protons interact with photons in the energy range  $\epsilon_{\gamma m}$  to  $\epsilon_{\gamma c}$ , where the photon spectrum  $L_\epsilon \propto \epsilon_\gamma^{1/2}$  and the number of photons above interaction threshold is  $\propto \epsilon_p^{1/2}$ . At lower energy, protons interact with photons of energy  $\epsilon_\gamma > \epsilon_{\gamma c}$ , where  $L_\epsilon \propto \epsilon^{-1}$  rather than  $L_\epsilon \propto \epsilon^{-1/2}$ . At these energies therefore  $f_\pi \propto \epsilon_p$ .

Since approximately half the energy lost by protons of energy  $\epsilon_p$  is converted to neutrinos with energy  $\sim 0.05\epsilon_p$ , Eq. (42) implies that the spectrum of neutrinos below  $\epsilon_{\nu b} \approx 10^{17}(\Gamma_{\text{tr.}}/250)^2(\epsilon_{\gamma c, \text{keV}})^{-1}\text{eV}$  is harder by one power of the energy than the proton spectrum, and by half a power of the energy at higher energy. For a power law differential spectrum of accelerated protons  $dn_p/d\epsilon_p \propto \epsilon_p^{-2}$ , the differential neutrino spectrum is  $dn_\nu/d\epsilon_\nu \propto \epsilon_\nu^{-\alpha}$  with  $\alpha = 1$  below the break and  $\alpha = 3/2$  above the break. Assuming that GRBs are indeed the sources of ultra-high energy cosmic rays, then Eqs. (41,42) and (24) imply that the expected neutrino intensity is

$$\begin{aligned} \epsilon_\nu^2 \Phi_{\nu_\mu} &\approx \epsilon_\nu^2 \Phi_{\bar{\nu}_\mu} \approx \epsilon_\nu^2 \Phi_{\nu_e} \\ &\approx 10^{-10} \frac{f_\pi^{[19]}}{0.1} \left( \frac{\epsilon_\nu}{10^{17}\text{eV}} \right)^\beta \text{GeV cm}^{-2}\text{s}^{-1}\text{sr}^{-1}, \end{aligned} \quad (43)$$

where  $f_\pi^{[19]} \equiv f_\pi(\epsilon_{p,20} = 2)$  and  $\beta = 1/2$  for  $\epsilon_\nu > 10^{17}\text{eV}$  and  $\beta = 1$  for  $\epsilon_\nu < 10^{17}\text{eV}$ .

Some GRBs may result from the collapse of a massive star, in which case the fireball is expected to expand into a pre-existing wind (e.g. [22,118]). For typical wind parameters, the transition to self-similar behavior takes place at a radius where the wind density is  $n \approx 10^4\text{cm}^{-3} \gg 1\text{cm}^{-3}$ . The higher density implies a lower Lorentz factor of the expanding plasma during the transition stage, and a larger fraction of proton energy lost to pion production. Protons of energy  $\epsilon_p \geq 10^{18}\text{eV}$  lose all their energy to pion production in this case. If most GRBs result from the collapse of massive stars, then the predicted neutrino flux is [111,26]

$$\epsilon_\nu^2 \Phi_\nu \approx 10^{-8} \min\{1, \epsilon_\nu^{\text{ob.}}/10^{17}\text{eV}\} \text{GeV cm}^{-2}\text{s}^{-1}\text{sr}^{-1}. \quad (44)$$

The neutrino flux is expected to be strongly suppressed at energy  $\epsilon_\nu > 10^{19}\text{eV}$ , since protons are not expected to be accelerated to energy  $\epsilon_p \gg 10^{20}\text{eV}$ . If protons are accelerated to much higher energy, the  $\nu_\mu$  ( $\bar{\nu}_\mu$ ,  $\nu_e$ ) flux may extend to  $\sim 10^{21}n_0^{-1/2}\xi_{B,-1}^{-1/2}\text{eV}$  ( $\sim 10^{20}n_0^{-1/2}\xi_{B,-1}^{-1/2}\text{eV}$ ). At higher energy, synchrotron losses of pions (muons) will suppress the neutrino flux.

### 6.3 Inelastic $p$ - $n$ collisions

The acceleration,  $\gamma \propto r$ , of fireball plasma emitted from the source of radius  $r_0$  (see §2.2) is driven by radiation pressure. Fireball protons are accelerated through their coupling to the electrons, which are coupled to fireball photons. Fireball neutrons, which are expected to exist in most progenitor scenarios, are coupled to protons by nuclear scattering as long as the comoving  $p$ - $n$  scattering time is shorter than the comoving wind expansion time  $r/\gamma c = r_0/c$ . As the fireball plasma expands and accelerates, the proton density decreases,  $n_p \propto r^{-2}\gamma^{-1}$ , and neutrons may become decoupled. For  $\eta > \eta_{pn}$ , where

$$\eta_{pn} \approx 400L_{52}^{1/4}r_{0,7}^{-1/4}, \quad (45)$$

neutrons decouple from the accelerating plasma prior to saturation,  $\gamma = \eta$ , at  $\Gamma = \eta_{pn}^{4/3} \eta^{-1/3}$  [28,6]. In this case, relativistic relative velocities between protons and neutrons arise, which lead to pion production through inelastic nuclear collisions. Since decoupling occurs at a radius where the collision time is similar to wind expansion time, each  $n$  leads on average to one pair of  $\nu\bar{\nu}$ . The typical comoving neutrino energy,  $\sim 50$  MeV, implies an observed energy  $\sim 10$  GeV. A typical burst,  $E = 10^{53}$  erg at  $z = 1$ , with significant neutron to proton ratio and  $\eta > 400$  will therefore produce a fluence  $F(\nu_e + \bar{\nu}_e) \sim 0.5F(\nu_\mu + \bar{\nu}_\mu) \sim 10^{-4} \text{cm}^{-2}$  of  $\sim 10$  GeV neutrinos.

Relativistic relative  $p$ - $n$  velocities, leading to neutrino production through inelastic collisions, may also result from diffusion of neutrons between regions of the fireball wind with large difference in  $\Gamma$  [74]. If, for example, plasma expanding with very high Lorentz factor,  $\Gamma > 100$ , is confined to a narrow jet surrounded by a slower,  $\Gamma \sim 10$  wind, internal collisions within the slower wind can heat neutrons to relativistic temperature, leading to significant diffusion of neutrons from the slower wind into the faster jet. Such process may operate for winds with  $\eta < 400$  as well as for  $\eta > 400$ , and may lead, for certain (reasonable) wind parameter values, to  $\sim 10$  GeV neutrino flux similar to that due to  $p$ - $n$  decoupling in a  $\eta > 400$  wind.

#### 6.4 Implications

The high energy neutrinos predicted in the dissipative wind model of GRBs may be observed by detecting the Cerenkov light emitted by high energy muons produced by neutrino interactions below a detector on the surface of the Earth (see [39] for a recent review). The probability  $P_{\nu\mu}$  that a neutrino would produce a high energy muon in the detector is approximately given by the ratio of the high energy muon range to the neutrino mean free path. For the neutrinos produced in internal shocks,  $\epsilon_\nu \sim 10^{14}$  eV,  $P_{\nu\mu} \simeq 1.3 \times 10^{-6}(\epsilon_\nu/1\text{TeV})$  [39]. Using (37), the expected flux of neutrino induced muons is

$$J_\mu \approx 10 \frac{f_\pi(\epsilon_{pb})}{0.2} \text{km}^{-2} \text{yr}^{-1}. \quad (46)$$

The rate is almost independent of  $\epsilon_{\nu b}$ , due to the increase of  $P_{\nu\mu}$  with energy. The rate (46) is comparable to the background expected due to atmospheric neutrinos [39]. However, neutrino bursts should be easily detected above the background, since the neutrinos would be correlated, both in time and angle, with the GRB  $\gamma$ -rays. A  $\text{km}^2$  neutrino detector should detect each year  $\sim 10$  neutrinos correlated with GRBs. Note, that at the high energies considered, knowledge of burst direction and time will allow to discriminate the neutrino signal from the background by looking not only for upward moving neutrino induced muons, but also by looking for down-going muons.

The predicted flux of  $\sim 10^{17}$  eV neutrinos, produced by photo-meson interactions during the onset of fireball interaction with its surrounding medium,

Eqs. (43,44), may be more difficult to detect. For the energy range of after-glow neutrinos, the probability  $P_{\nu\mu}$  that a neutrino would produce a high energy muon with the currently required long path within the detector is  $P_{\nu\mu} \approx 3 \times 10^{-3}(\epsilon_\nu/10^{17}\text{eV})^{1/2}$  [39,41]. This implies, using (43), an expected detection rate of muon neutrinos of  $\sim 0.06/\text{km}^2\text{yr}$  (over  $2\pi$  sr), assuming fireballs explode in and expand into typical inter-stellar medium gas. If, on the other hand, most GRB progenitors are massive stars and fireballs expand into a pre-existing stellar wind, Eq. (44) implies a detection of several muon induced neutrinos per year in a  $1\text{km}^3$  detector. We note, that GRB neutrino detection rates may be significantly higher than derived based on the above simple arguments, because the knowledge of neutrino direction and arrival time may relax the requirement for long muon path within the detector.

Air-showers could be used to detect ultra-high energy neutrinos. The neutrino acceptance of the planned Auger detector,  $\sim 10^4\text{km}^3\text{sr}$  [19], seems too low. The effective area of proposed space detectors [65,94] may exceed  $\sim 10^6\text{km}^2$  at  $\epsilon_\nu > 2 \times 10^{19}$  eV, detecting several tens of GRB correlated events per year, provided that the neutrino flux extends to  $\epsilon_\nu > 2 \times 10^{19}$  eV. Since, however, the GRB neutrino flux is not expected to extend well above  $\epsilon_\nu \sim 10^{19}$  eV, and since the acceptance of space detectors decrease rapidly below  $\sim 10^{19}$  eV, the detection rate of space detectors would depend sensitively on their low energy threshold.

Detection of high energy neutrinos will test the shock acceleration mechanism and the suggestion that GRBs are the sources of ultra-high energy protons, since  $\geq 10^{14}$  eV ( $\geq 10^{18}$  eV) neutrino production requires protons of energy  $\geq 10^{16}$  eV ( $\geq 10^{19}$  eV). The dependence of  $\sim 10^{17}$  eV neutrino flux on fireball environment imply that the detection of high energy neutrinos will also provide constraints on GRB progenitors.

Inelastic  $p$ - $n$  collisions may produce  $\sim 10$  GeV neutrinos with a fluence of  $\sim 10^{-4}\text{cm}^{-2}$  per burst, due to either  $p$ - $n$  decoupling in a wind with high neutron fraction and high,  $> 400$ , Lorentz factor [28,6], or to neutron diffusion in a wind with, e.g., strong deviation from spherical symmetry [74]. The predicted number of events in a  $1\text{km}^3$  neutrino telescope is  $\sim 10\text{yr}^{-1}$ . Such events may be detectable in a suitably densely spaced detector. Detection of  $\sim 10$  GeV neutrinos will constrain the fireball neutron fraction, and hence the GRB progenitor.

Detection of neutrinos from GRBs could be used to test the simultaneity of neutrino and photon arrival to an accuracy of  $\sim 1$  s ( $\sim 1$  ms for short bursts), checking the assumption of special relativity that photons and neutrinos have the same limiting speed. These observations would also test the weak equivalence principle, according to which photons and neutrinos should suffer the same time delay as they pass through a gravitational potential. With 1 s accuracy, a burst at 100 Mpc would reveal a fractional difference in limiting speed of  $10^{-16}$ , and a fractional difference in gravitational time delay of order  $10^{-6}$  (considering the Galactic potential alone). Previous applications of these ideas to supernova 1987A (see [5] for review), where simultaneity could be checked only to an accuracy of order several hours, yielded much weaker upper limits:

of order  $10^{-8}$  and  $10^{-2}$  for fractional differences in the limiting speed and time delay respectively.

The model discussed above predicts the production of high energy muon and electron neutrinos. However, if the atmospheric neutrino anomaly has the explanation it is usually given, oscillation to  $\nu_\tau$ 's with mass  $\sim 0.1$  eV [21,37,33], then one should detect equal numbers of  $\nu_\mu$ 's and  $\nu_\tau$ 's. Up-going  $\tau$ 's, rather than  $\mu$ 's, would be a distinctive signature of such oscillations. Since  $\nu_\tau$ 's are not expected to be produced in the fireball, looking for  $\tau$ 's would be an "appearance experiment." To allow flavor change, the difference in squared neutrino masses,  $\Delta m^2$ , should exceed a minimum value proportional to the ratio of source distance and neutrino energy [5]. A burst at 100 Mpc producing  $10^{14}$ eV neutrinos can test for  $\Delta m^2 \geq 10^{-16}$ eV<sup>2</sup>, 5 orders of magnitude more sensitive than solar neutrinos.

*Acknowledgments.* This work was supported in part by grants from the Israel-US BSF (BSF-9800343), MINERVA, and AEC (AEC-38/99). EW is the Incumbent of the Beracha foundation career development chair.

## References

1. Aharonian, F. A., & Cronin, J. W., Phys. Rev. D **50**, 1892 (1994).
2. Akerlof, C. W. *et al.*, Nature, **398**, 400 (1999).
3. Alvarez-Muniz, J., Halzen, F., & Hooper, D. W., Phys. Rev. **D62**, 093015 (2000).
4. Axford, W. I., Leer, E., & Skadron, G., Proc. 15th Int. Conf. Cosmic Rays, Plovdiv, Bulgaria (1977).
5. Bahcall, J. N., *Neutrino Astrophysics*, Cambridge University Press (NY 1989), pp. 438–460.
6. Bahcall, J. N., & Mészáros, Phys. Rev. Lett., 85, 1362 (2000).
7. Bahcall, J. N., & Waxman, E., Ap. J. **542**, 542 (2000).
8. Band, D., *et al.*, Ap. J. **413**, 281 (1993).
9. Baring, M., Ap. J. **418**, 391 (1993).
10. Bell, A. R., MNRAS **182**, 147 (1978).
11. Bhat, P. N., *et al.*, Nature **359**, 217 (1992);
12. Bird, D. J., *et al.*, Phys. Rev. Lett. **71**, 3401 (1993).
13. Bird, D. J., *et al.*, Ap. J. **424**, 491 (1994).
14. Blandford, R., & Eichler, D., Phys. Rep. **154**, 1 (1987).
15. Blandford, R. D., & Mckee, C. F., Phys. Fluids **19**, 1130 (1976).
16. Blandford, R. D., & Ostriker, J. P., Ap. J. **221**, L229 (1978).
17. Boyle, B. J. & Terlevich, R. J., MNRAS **293**, L49 (1998).
18. Brainerd, J. J. *et al.*, Proc. 19th Texas Symposium on Relativistic Astrophysics and Cosmology (Paris, 1998).
19. Capelle, K. S., Cronin, J. W., Parente, G., & Zas, E. Astropar. Phys. **8**, 321 (1998).
20. Cargill, P. J. & Papadopoulos K., Ap. J., **329**, L29 (1988).
21. D. Casper *et al.*, Phys. Rev. Lett. **66**, 2561 (1991).
22. Chevalier, R. A., & Li, Z., Ap. J., **536**, 195 (2000).
23. Corbató, S. C. *et al.*, Nuc. Phys. **28B** (Proc. Suppl.), 36 (1992); see also <http://www.physics.adelaide.edu.au/astrophysics/FlysEye.html>
24. Costa, E. *et al.*, Nature **387**, 783 (1997).
25. Cronin, J. W., Nucl. Phys. B (Proc. Suppl.) **28B**, 213 (1992).

26. Dai, Z. G., & Lu, T., submitted to Ap. J. (astro-ph/0002430).
27. Dawson, B. R., Meyhandan, R., Simpson, K.M., *Astropart. Phys.* **9**, 331 (1998).
28. Derishev, E. V., Kocharovsky, V. V., & Kocharovsky, V. V., *Ap. J.* **521**, 640 (1999).
29. Dermer, C. D., submitted to Ap. J. (astro-ph/0005440).
30. Efimov, N. N. *et al.*, in *Proceedings of the International Symposium on Astrophysical Aspects of the Most Energetic Cosmic-Rays*, edited by M. Nagano and F. Takahara (World Scientific, Singapore, 1991), p. 20.
31. Fishman, G. J., *et al.*, *Ap. J. Supp.* **92**, 229 (1994).
32. Fishman, G. J. & Meegan, C. A., *ARA&A* **33**, 415 (1995).
33. Fogli, G. L., & Lisi E., *Phys. Rev.* **D52**, 2775 (1995).
34. Frail, D., Waxman, E. & Kulkarni, S., *Ap. J.* **537**, 191 (2000).
35. Freedman, D. L., & Waxman, E., *Ap. J.* **547**, 922 (2001).
36. Fryer, C. L. & Woosley, S. E., *Ap. J.* **502**, L9 (1998).
37. Y. Fukuda *et al.*, *Phys. Lett.* **B335**, 237 (1994);
38. Gaissner, T. K. *et al.*, *Phys. Rev.* **D47**, 1919 (1993).
39. Gaissner, T. K., Halzen, F., & Stanev, T., *Phys. Rep.* **258**, 173 (1995).
40. Gallant, Y. A., & Achterberg, A., *MNRAS* **305**, L6 (1999).
41. Gandhi, R., Quigg, C., Reno, M., & Sarcevic, I., *Phys. Rev.* **D58**, 093009 (1998).
42. Goodman, J., *Ap. J.* **308**, L47 (1986).
43. Greisen, K., *Phys. Rev. Lett.* **16**, 748 (1966).
44. Guetta, D., Spada M., & Waxman, E., to appear in *Ap. J.* (astro-ph/0011170).
45. Guetta, D., Spada M., & Waxman, E., submitted to *Ap. J.* (astro-ph/0102487).
46. Halzen, F., in *Proc. 17th International Workshop on Weak Interactions and Neutrinos* (Cape Town, South Africa, January 1999) (astro-ph/9904216).
47. Halzen, F. & Hooper, D. W., *Ap. J.* **527**, L93 (1999).
48. Hayashida, N. *et al.*, *Phys. Rev. Lett.* **73**, 3491 (1994);
49. Hayashida, N. *et al.*, *Astrophys. J.* **522**, 225 (1999) and astro-ph/0008102.
50. Helfand, D. J. & Becker, R. H., *Ap. J.*, **314**, 203 (1987).
51. Hewett, P. C., Foltz, C. B. & Chaffee, F., *Ap. J.* **406**, 43 (1993).
52. Hillas, A. M., *ARA&A* **22**, 425 (1984).
53. Hogg, D. W. & Fruchter, A. S., *Ap. J.* **520**, 54 (1999).
54. Katz, J. I., *Ap. J.* **432**, L107 (1994).
55. Kippen, R. M., to appear in *Proc. Second Rome Workshop: Gamma-Ray Bursts in the Afterglow Era* (Rome, 2000) (astro-ph/0201277).
56. Koyama, K. *et al.*, *Nature* **378**, 255 (1995).
57. Krolik, J. H. & Pier, E. A., *Ap. J.* **373**, 277 (1991).
58. Kronberg, P. P., *Rep. Prog. Phys.* **57**, 325 (1994).
59. Kronberg, P. P., Reinhardt, M. & Simard-Normandin, M., *A&A* **61**, 771 (1977).
60. Krumholz, M., Thorsett, S. E., & Harrison, F. A., *Ap. J.* **506**, L81 (1998).
61. Kulkarni, S. R. *et al.*, To appear in *Proc. of the 5th Huntsville Gamma-Ray Burst Symposium* (astro-ph/0002168).
62. Kulsrud, R. M., in *Particle Acceleration Mechanisms in Astrophysics*, eds. J. Arons, C. Max, and C. McKee (AIP 56, NY 1979).
63. Lemoine, M., Sigl, G., Olinto, A. V. & Schramm, D. N., *Ap. J.* **486**, L115 (1997).
64. Lilly, S. J. , Le Fevre, O., Hammer F., & Crampton, D., *Ap. J.* **460**, L1 (1996).
65. Linsley, J. 1985, *Proc. 19th Intl. Cosmic-Ray conference*, 3, 438
66. Livio, M. & Waxman, E., *Ap. J.* **538**, 187 (2000).
67. Madau, P., *et al.* *MNRAS* **283**, 1388 (1996).
68. Mao, S. & Mo, H. J., *A&A* **339**, L1 (1998).
69. Mészáros, P., in *Proc. 17th Texas Conf. Relativistic Astrophysics*, *Annals Ny. Acad. Sci.* No. 759 (NY Acad. Sci., NY 1995).

70. Mészáros, P., A&AS **138**, 533 (1999).
71. Mészáros, P., & Rees, M., MNRAS **269**, 41P (1994).
72. Mészáros, P. & Rees, M., Ap. J. **476**, 232 (1997).
73. Mészáros, P. & Rees, M., MNRAS **306**, L39 (1999).
74. Mészáros, P., & Rees, M., Ap. J. **541**, L5 (2000).
75. Milgrom, M. & Usov, V., Ap. J. **449**, L37 (1995).
76. Miralda-Escudé, J. & Waxman, E., Ap. J. **462**, L59 (1996).
77. Mücke, A. *et al.*, Pub. Astron. Soc. Australia **16**, 160 (1999).
78. Narayan, R., Paczyński, B., & Piran, T., Ap. J. **395**, L83 (1992).
79. Paczyński, B., Ap. J. **308**, L43 (1986).
80. Paczyński, B., Ap. J. **363**, 218 (1990).
81. Paczynski, B., in *Gamma Ray Bursts: 4th Huntsville Symp.*, eds. C. A. Meegan, R. D. Pierce, & T. M. Koshut (Woodbury: AIP), 783 (1998).
82. Paczyński, B. & Rhoads, J., Ap. J. **418**, L5 (1993).
83. Paczyński, B. & Xu, G., Ap. J. **427**, 708 (1994).
84. Piran, T., Phys. Rep. **333**, 529 (2000).
85. Rachen, J. P., & Mészáros, P., Proc. 4th Huntsville Symposium on GRBs, 1998 (AIP Conf. Proc. **428**, Gamma Ray Bursts), p. 776.
86. Rachen, J. P., & Mészáros, P., Phys. Rev. D **58**, 123005 (1998).
87. Rees, M. & Mészáros, P., MNRAS **258**, 41P (1992).
88. Sari, R., & Piran, T., Ap. J. **485**, 270 (1997).
89. Sari, R. & Piran, T., Ap. J. **517**, L109 (1999).
90. Schmidt, M., Schneider, D. P., & Gunn, J. E., Astron. J. **110**, 68 (1995).
91. Shemi, A., & Piran, T., Ap. J. **365**, L55 (1990).
92. Sigl, G., Lemoine, M. & Olinto, A. V., Phys. Rev. **D56**, 4470 (1997).
93. Sommer, M. *et al.*, Ap. J. **422**, L63 (1994).
94. Takahashi, Y. 1995, Proc. 24th Intl. Cosmic-Ray conference, 3, 595
95. Takeda, M. *et al.*, Phys. Rev. Lett. **81**, 1163 (1998).
96. Takeda, M. *et al.*, Ap. J. **522**, 225 (1999).
97. Teshima, M. *et al.*, Nuc. Phys. **28B** (Proc. Suppl.), 169 (1992); see also <http://www-ta.icrr.u-tokyo.ac.jp/>
98. Totani, T., A&AS **142**, 443 (2000).
99. Vietri, M., Ap. J. **453**, 883 (1995).
100. Vietri, M., Ap. J. **478**, L9 (1997).
101. Vietri, M., Phys. Rev. Lett. **80**, 3690 (1998).
102. Watson, A. A., Nucl. Phys. B (Proc. Suppl.) **22B**, 116 (1991).
103. Watson, A. A., in Nuclear and Particle Phys. 1993, eds. MacGregor, I. J. D. & Doyle, A. T. (Inst. Phys. Conf. Ser. **133**) (Bristol:IoP), 135; see also <http://www.auger.org/>
104. Waxman, E., Phys. Rev. Lett. **75**, 386 (1995).
105. Waxman, E., Ap. J. **452**, L1 (1995).
106. Waxman, E., Ap. J. **485**, L5 (1997).
107. Waxman, E. Ap. J. **491**, L19 (1997).
108. Waxman, E., Nucl. Phys. B (Proc. Suppl.) **87**, 345 (2000).
109. Waxman, E., & Bahcall, J. N., Phys. Rev. Lett. **78**, 2292 (1997).
110. Waxman, E., & Bahcall, J. N., Phys. Rev. **D59**, 023002 (1999).
111. Waxman, E., & Bahcall, J. N., Ap. J. **541**, 707 (2000).
112. Waxman, E., & Coppi, P., Ap. J. **464**, L75 (1996).
113. Waxman, E. & Draine, B. T., Ap. J. **537**, 796 (2000).
114. Waxman, E., Kulkarni, S. & Frail, D., Ap. J. **497**, 288 (1998).



115. Waxman, E. & Miralda-Escudé, J., *Ap. J.* **472**, L89 (1996).
116. Wijers, A. M. J., Rees, M. J. & Mészáros, P., *MNRAS* **288**, L51 (1997).
117. Woods, E. & Loeb, A., *Ap. J.* **453**, 583 (1995).
118. Woosley, S. E., & MacFadyen, A. I., *A&AS*, **138**, 499 (1999).
119. Yoshida, S., *et al.*, *Astropar. Phys.* **3**, 151 (1995).
120. Zatsepin, G. T., & Kuzmin, V. A., *JETP lett.*, **4**, 78 (1966).